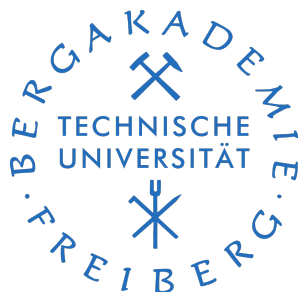


# **Development and implementation of user material subroutines for fibre reinforced plastics in a commercial FEM software**

**Master thesis**



Presented by: Arun Prakash Ganapathy

Matriculation number: 63876

Course: Computational Materials Science (CMS)

Institute of Mechanics and Fluid Dynamics

First Examiner: Prof. Dipl.-Ing. Björn Kiefer, Ph.D.

Second Examiner: Dr.-Ing. Stephan Roth

Betreuer: Dr.-Ing. Andreas Seupel

External supervisor: Dr.-Ing. Dominik Laveuve  
Fraunhofer-Institut für Betriebsfestigkeit  
und Systemzuverlässigkeit (LBF)

TU Bergakademie Freiberg

August 2021



# Abstract

Composite materials especially fibre-reinforced plastics are replacing conventional material like metals because of their superior strength and light-weight properties not only in advanced structural components but also in everyday life. Fraunhofer LBF specializes on safety and reliability of sustainable, light-weight structures. So numerical and experimental analysis and efficient manufacturing of fibre-reinforced plastics play an important role in the design and development of light-weight, sustainable and reliable components. Therefore the ongoing project at Fraunhofer LBF investigates the fatigue and creep behaviour of short fibre-reinforced thermoplastics. The main aim of this master thesis is to develop progressive damage models which can predict the initiation and propagation of damage once the material exceeds its failure strength. The constitutive equations necessary for simulating the behaviour of damaged materials are established in the framework of continuum damage mechanics (CDM). Because of the complex material behaviour of the composite materials, anisotropic damage mechanism is employed to represent the distribution of damage. Non-linear damage evolution law based on fracture energy regularization technique is applied to represent the damage evolution. First the orthotropic behaviour (Linear-elastic) of the composite materials and the anisotropic damage models are implemented and tested at integration point levels. After that, representative structural examples are used to test the damage models and analyse how they behave in various loading conditions. The global force-displacement response is analysed to address the issue related to numerical implementation such as convergence, mesh sensitivity during strain-softening etc., Finally the distribution of damage at the end of loading process is plotted to visualize the damage propagation in a composite material under loading.



# Acknowledgement

I would like to express my sincere thanks to Dr.-Ing. Dominik Laveuve for his guidance, support and timely feedbacks throughout this master thesis work. I would like to extend my gratitude to Prof.Dr.-Ing.Björn Kiefer for providing me the chance to pursue this thesis work under his supervision and Dr.-Ing. Andreas Seupel for his valuable insights through out the thesis work. I would like to thank Fraunhofer LBF for this opportunity and providing me with the required resources for completion of this thesis work. Last but not least, I am thankful to my friends and family for their constant moral support.



# **Declaration**

Hereby, I formally declare that I have developed and written the enclosed thesis without illegitimate help of a third party and that no other than the indicated aids have been used for its completion; all thoughts from other sources that have been used literally or indirectly are marked as such. The thesis has not been submitted to any other examination committee in this or a similar form.

Arun Prakash Ganapathy

.....

Freiberg, 30.08.2021



# Contents

<b>Contents</b>	<b>VII</b>
<b>List of Figures</b>	<b>XI</b>
<b>List of Tables</b>	<b>XV</b>
<b>List of symbols</b>	<b>XVII</b>
<b>1 Introduction</b>	<b>1</b>
1.1 Background and motivation . . . . .	1
1.2 Scope and Outline . . . . .	3
<b>2 Continuum damage mechanics</b>	<b>7</b>
2.1 Damage . . . . .	7
2.2 Representative Volume Element(RVE) . . . . .	8
2.3 Concept of continuum damage mechanics (CDM) . . . . .	9
2.3.1 Modelling by Effective area reduction . . . . .	9
2.3.2 Modelling by variation of elastic modulus . . . . .	10
2.4 Mechanical representation of the damage state . . . . .	11
2.4.1 Scalar damage variable . . . . .	11
2.4.2 Vector damage variable . . . . .	12
2.4.3 Damage tensor of second order . . . . .	12
2.5 Effective Stress Tensors . . . . .	13
2.5.1 Effective stress tensor for isotropic damage (Lemaitre and Chaboche, 1978) . . . . .	13
2.5.2 Asymmetric effective stress tensor for anisotropic damage (Murakami, 2012) . . . . .	13
2.5.3 Symmetrized effective stress tensor for anisotropic damage (Murakami, 2012) . . . . .	14
2.6 Damage effect tensors . . . . .	14
2.7 Hypothesis of strain Equivalence . . . . .	15
2.8 Hypothesis of strain energy equivalence . . . . .	16

2.9	Elastic constitutive equation and elastic modulus tensor of orthotropic material . . . . .	18
<b>3</b>	<b>Working environment</b>	<b>21</b>
3.1	Software tools required . . . . .	21
3.2	Programming the USERMAT . . . . .	22
3.3	Compiling the USERMAT . . . . .	23
3.4	Creating FE model . . . . .	24
3.5	Testing the USERMAT . . . . .	25
3.6	PostProcessing . . . . .	26
<b>4</b>	<b>Progressive failure analysis of orthotropic composite materials</b>	<b>27</b>
4.1	Fibre-reinforced Composites . . . . .	27
4.1.1	Longitudinal failure . . . . .	27
4.1.2	Transverse failure . . . . .	28
4.2	Damage initiation criteria . . . . .	28
4.2.1	3D Hashin's quadratic strain criteria . . . . .	28
4.2.2	Maximum stress criteria . . . . .	29
4.2.3	Modified Hashin's failure criterion . . . . .	30
4.3	Types of damage evolution . . . . .	31
4.3.1	Isotropic damage . . . . .	31
4.3.2	Anisotropic damage . . . . .	32
4.4	Localisation and Mesh Regularisation . . . . .	33
4.5	Numerical implementation of the damage model in ANSYS . . . . .	34
4.5.1	Strain based damage model . . . . .	35
4.5.2	Stress based damage model . . . . .	36
4.6	Schematic of UMAT implementation . . . . .	37
<b>5</b>	<b>Results and Discussion</b>	<b>39</b>
5.1	Modelling linear elastic behaviour of orthotropic materials . . . . .	39
5.2	Damage behaviour at integration point level . . . . .	42
5.2.1	Uniaxial tension . . . . .	42
5.2.2	Biaxial tension . . . . .	48
5.2.3	Triaxial tension . . . . .	49
5.3	Representative structural examples . . . . .	51
5.3.1	Notched tensile specimen . . . . .	53
5.3.2	Compact Tension (CT) Specimen . . . . .	58
5.3.3	Plate with hole (3D) . . . . .	66
<b>6</b>	<b>Summary and Conclusion</b>	<b>71</b>
<b>Bibliography</b>		<b>73</b>

<b>Appendix</b>	<b>XVIII</b>
A.1 Elastic stiffness matrix of the damaged material . . . . .	XVIII
A.1.1 Plane stress (2D) . . . . .	XVIII
A.1.2 3D . . . . .	XVIII

X

# List of Figures

1.1	Composite materials used in a Boeing 787 'Dreamliner' (P.Nikethan, 2016) . . . . .	1
1.2	Strain-softening of composite materials after damage initiation (Rafi et al., 2007) . . . . .	2
2.1	Scales of damage observation (Murakami, 2012) . . . . .	8
2.2	Effective area reduction due to microcracks (Murakami, 2012) . . . .	9
2.3	Damage of bar under tensile load (Murakami, 2012) . . . . .	10
2.4	Surface element in RVE of a damaged material (Murakami, 2012) . .	12
2.5	Hypothesis of strain equivalence (Murakami, 2012) . . . . .	16
2.6	Hypothesis of strain energy equivalence (Murakami, 2012) . . . . .	17
3.1	USERMAT Interface (Lin, 1999) . . . . .	23
3.2	Table (TB) commands . . . . .	25
3.3	Time history post processor window . . . . .	26
4.1	Fracture planes in FRP material (Maimí et al., 2007) . . . . .	28
4.2	Types of degradation behaviour in damaged composite materials (Wang et al., 2009) . . . . .	31
5.1	Stress-Strain relation (Standard vs user-defined material routine) . .	39
5.2	Contour plots of the stress components $\sigma_{11}$ , $\sigma_{22}$ and $\sigma_{33}$ of the bar obtained using standard (Figures a,c,e on the left) and user-defined material routine (Figures b, d, f on the right) . . . . .	41
5.3	Evolution of stress for uniaxial tension test in 11 direction . . . . .	43
5.4	Evolution of damage components for uniaxial tension test in 11 direction	43
5.5	Influence of softening parameter $P$ in the damage evolution) . . . .	44
5.6	Convergence issue: Residual norm of the stress vs No of Newton- raphson iterations . . . . .	45
5.7	Evolution of stress and damage components with stress-based damage initiation criteria under uniaxial tension . . . . .	46
5.8	Influence of element volume ( $V$ ) on the damage evolution . . . . .	47
5.9	The strain components $\epsilon_{22}$ and $\epsilon_{33}$ computed using algorithmic (a) and numerical tangent stiffness (b) under uniaxial tension . . . . .	48

5.10 Evolution of stress (Figures a, c on the left) and corresponding damage (Figure b, d on the right) components under biaxial tension . . . . .	49
5.11 Evolution of stress (Figures a, c, e on the left) and corresponding (Figures b ,d, f on the right) damage components under triaxial tension	50
5.12 Specimen geometry and boundary conditions. Dimensions are given in mm. Displacement controlled loading $U_x$ is applied. . . . .	53
5.13 Considered meshes (h is the length of the element along fracture zone and n the total number of elements) . . . . .	54
5.14 Convergence study: Global force-displacement response for model with regularization (Figure a on the left) and without regularization (Figure b the right) . . . . .	54
5.15 Convergence study for model with(Figure a,c,e) and without(b,d,f) regularization: Damage contour plots $d_1$ at the end of the loading . .	56
5.16 Damage contour plots $d_2$ at the end of the loading (Loading in transverse direction) . . . . .	57
5.17 Comparison of force-displacement response in longitudinal and transverse direction for h=0.5mm discretization . . . . .	57
5.18 Specimen geometry and boundary conditions. Dimensions are given in mm. Displacement controlled loading $U_x$ is applied . . . . .	58
5.19 Considered meshes (h is the length of the element along fracture zone and n the total number of elements) . . . . .	59
5.20 Convergence study: Global force-displacement response for three different meshes . . . . .	60
5.21 Damage distributions at the end of loading in longitudinal direction: Damage contour plots $d_1$ and $d_2$ . . . . .	61
5.22 Damage distributions at the end of loading in transverse direction: Damage contour plots $d_1$ and $d_2$ (h = 1mm discretization) . . . . .	61
5.23 Comparison of force-displacement response in longitudinal and transverse direction for h = 1 mm discretization . . . . .	62
5.24 Comparison of force-displacement response for different shear co-efficient ( $\alpha$ ) (h= 1mm discretization) . . . . .	62
5.25 Evolution of stress components during longitudinal tensile loading (h= 1mm discretization) . . . . .	63
5.26 Damage distributions at the end of longitudinal loading: Damage contour plots $d_2$ for different shear co-efficients ( $\alpha$ ) . . . . .	64
5.27 Evolution of stress components during transverse tensile loading (h= 1mm discretization) . . . . .	65
5.28 Damage distributions at the end of transverse loading: Damage contour plots $d_1$ for different shear co-efficient ( $\alpha$ ) . . . . .	65
5.29 Specimen geometry and boundary conditions. Dimensions are given in mm. Displacement controlled loading $U_x$ is applied . . . . .	66

5.30	Finite element discretization used for 3D damage study . . . . .	67
5.31	Global force-displacement response for the longitudinal tensile load- ing . . . . .	68
5.32	Contour plots of the damage distribution $d_1$ , $d_2$ and $d_3$ at the end of longitudinal tensile loading . . . . .	70



# List of Tables

4.1	Maximum stress criterion . . . . .	30
5.1	Material parameters (Integration point studies) . . . . .	40
5.2	Material parameters (Representative structural examples) . . . . .	52
5.3	Material parameters (3D Damage model) . . . . .	67



# List of symbols

# Chapter 1

## Introduction

### 1.1 Background and motivation

Composite materials are made of two or more dissimilar materials of different physical, chemical or mechanical properties, which, when combined, create a material with properties unlike the individual constituent materials. One of the earliest use of composite materials date back to 3400 B.C when Mesopotamians glued wood strips at different angles to create plywood (TWI, 2016). Now a days advanced composite materials are widely used in structural design in various industries such as aerospace, automobile, marine, petrochemical etc., due to their superior properties over traditional engineering materials.

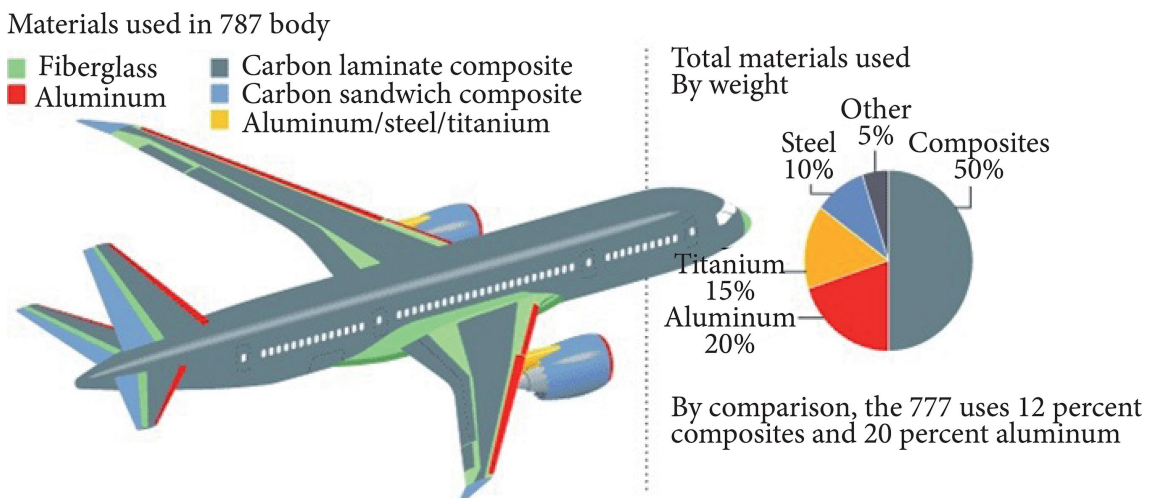


Figure 1.1: Composite materials used in a Boeing 787 'Dreamliner' (P.Nikethan, 2016)

Composite materials are attractive because of their high strength, high stiffness-to-density ratio, light weight properties etc. (Lapczyk and Hurtado, 2007), Another important reason for using composite materials is the possibility to tailor

the stiffness and strength to specific load applications flexibly (Wang et al., 2009). Despite their superior physical properties, composite materials can be damaged from a number of sources, both during initial processing and in operation. Since composite materials have complex material response and a low margin of safety through ductility as offered by metals, the development of damage must be understood for predicting failure of such materials (Lapczyk and Hurtado, 2007). For example fibre-reinforced plastics exhibit local damage such as fibre breakage, matrix cracking, fibre matrix debonds etc., under normal operating conditions which may contribute to the failure (Maimí et al., 2007). Therefore the ability to predict the initiation and growth of damage is important for predicting the performance, safety and reliability of the composite materials for commercial use.

Several methods have been proposed to analyze the failure of composite materials. The simplest of them is to degrade the stiffness of the material instantaneously using a degradation factor once the failure criteria is met (El-Sisi et al., 2015). While easy to implement, the sudden complete failure of the material does not agree well with the real-life behaviour. Progressive failure analysis of composite materials is required to predict the real-life mechanical behaviour under various loading conditions. Over the last few decades continuum damage mechanics (CDM) first proposed by (Kachanov, 1986), has been employed to analyse the progressive degradation of the materials. The CDM approach provides a methodology which can determine the full range of deterioration of the material starting from no damage to the fully disintegrated material.

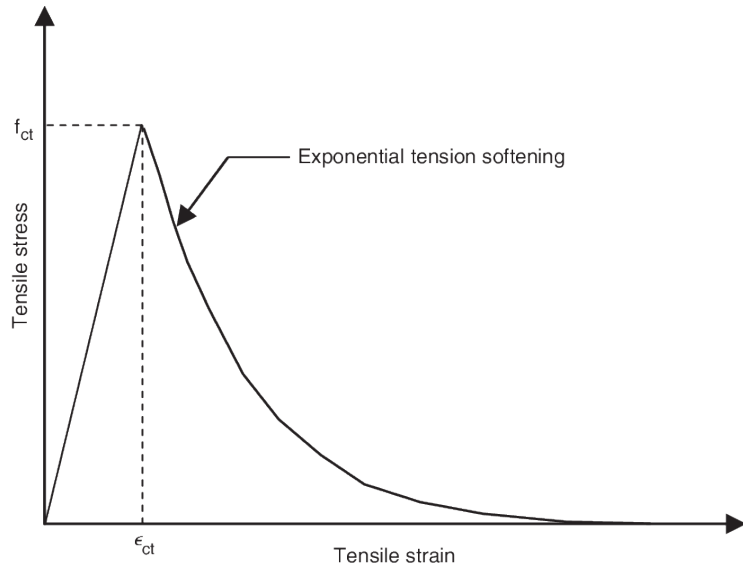


Figure 1.2: Strain-softening of composite materials after damage initiation (Rafi et al., 2007)

In CDM the damage is represented as a set of damage variables which describes

the current state of the material, and their development using set of evolution laws. Once the failure criteria is met, the damage variables are calculated using these evolution laws and the stiffness of the material is degraded with the help of the damage variables (Murakami, 2012) i.e., the material experiences strain-softening rather than strain-hardening observed in metals Figure (1.2). The very fact that the damage can be represented as a set of variables, makes them suitable for numerical simulations. Damage formulations can be easily fitted into non-linear finite element (FE) algorithms with the help of constitutive relations and implemented in simulation codes without the need to rely on special discretization techniques (Peerlings, 1999).

## 1.2 Scope and Outline

The objective of the thesis is to develop progressive damage models for predicting the initiation and propagation of damage in an orthotropic material when subjected to various loading conditions. Continuum damage mechanics (CDM) provides the framework for developing these damage models. Since the composite materials are orthotropic in nature i.e., they exhibit different material properties in mutually perpendicular directions, the model essentially consists of linear elasticity extended with an anisotropic damage mechanism. Therefore one damage variable is assigned to each principal material direction to represent the development of damage i.e., 2 damage variables are required when the problem is in 2D/Plane-stress and 3 variables when the problem is in 3D. The numerical modelling of the strain-softening behaviour results in strong mesh dependency which results in convergence issues when the mesh is refined (Wang et al., 2009). To reduce the mesh sensitivity, the fracture energy approach is used which includes fracture energy in the damage evolution laws. This ensures the objectivity of the model by adjusting the energy dissipated by each failure mechanism using a characteristic element length (Falzon and Apruzzese, 2011).

The stages of the thesis work are briefly described as follows

**Chapter 2** introduces the theoretical framework of continuum damage mechanics (CDM), constitutive relations and constitutive equations necessary for developing orthotropic material model.

**Chapter 3** gives reader a brief introduction into software used and the instructions to develop, compile and implement a material model in an FE environment.

**Chapter 4** gives a brief introduction to the mechanisms of damage and the different types of failure criteria and evolution equations necessary for developing damage models. In the end, the chapter deals with regularization technique used to reduce

mesh sensitivity problems and a brief description of how to implement the damage models numerically in a programming software.

**Chapter 5** The results of the finite element simulations are discussed in this chapter. Starting with the implementation of linear elastic behaviour of the orthotropic material the chapter discusses the behaviour of the damage models at integration point level and also using representative structural examples.





# Chapter 2

## Continuum damage mechanics

Continuum damage mechanics (CDM) is a theory for analyzing fracture and damage processes in materials from a continuum mechanics point of view. (CDM) provides a continuum perspective for microflaws initiation, propagation, and their coalescence that results in macroscopic damage and fractures. CDM uses state variables to represent the damage effect on the stiffness and remaining life of the material that is deteriorating as a result of load and ageing. A damage activation function is required to predict the initiation of damage and evolution laws are required to represent the propagation of damage in material subjected to load (Murakami, 2012).

### 2.1 Damage

Consider a body  $B$  of where a crack of length  $a$  has developed when subjected to an external load  $F$  as shown in Figure. 2.1 . A number of microcracks would be observed around the region arbitrary point  $P(x)$  near the crack tip. These microcracks are usually developed due to breakage of atomic bonds, or defects in the atomic array (Murakami, 2012). From the microscopic point of view, fracture of materials is a process of nucleation of microcracks due to the breakage of atomic bonds. From the macroscopic point of view, it is a process of extension of cracks brought about by the coalescence of these microcracks.

From the mesoscopic point of view, which exists between microscopic and macroscopic scale, it is a process of nucleation, growth and the coalescence of microscopic cavities that leads to the initiation of macroscopic crack. The development of microscopic, mesoscopic and macroscopic processes of fracture in materials and the resulting deterioration in their mechanical properties is called damage. Continuum damage mechanics aims to analyse the damage development during mesoscopic and macroscopic fracture processes in the framework of continuum mechanics (Murakami, 2012).

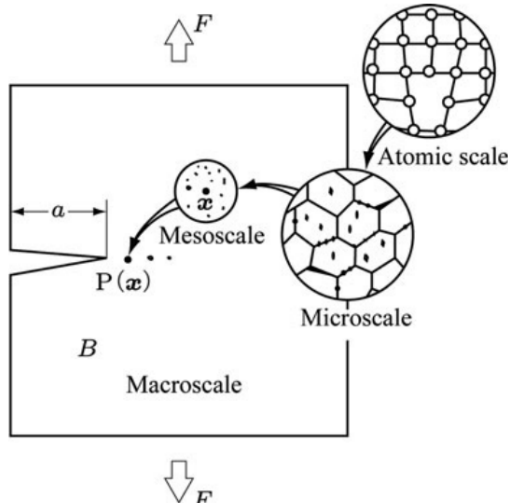


Figure 2.1: Scales of damage observation (Murakami, 2012)

## 2.2 Representative Volume Element(RVE)

To discuss the effects of microcracks in a material using CDM one must homogenize the mechanical effects of microstructure and represent them as a macroscopic continuous field in the material. For this purpose, we take a small region of a mesoscale around the material point  $P(x)$  in body  $B$ , as shown in Figure. 2.1. We assume that the material with discontinuities in this region as homogeneous, and the state of the material in this region can be represented by the statistical average of the mechanical variables in that region. This region is said to be the Representative Volume Element (RVE) (Hill, 1963) and (Hashin, 1983). For such RVE, the following two conditions must be satisfied (Murakami, 2012):

- For the material in the RVE to be homogeneous, the RVE should be sufficiently large enough to contain a number of discontinuities
- To represent a non-uniform macroscopic field by means of a continuum, the RVE size should be small enough so that the variation of the macroscopic variable in it may be insignificantly small

The size of RVE depends on the microstructure of the relevant material and their typical sizes are as follows (Lemaitre, 2012)

- Metals and ceramics -  $0.1 \text{ mm}^3$
- Polymers and composites -  $1 \text{ mm}^3$
- Timber -  $10 \text{ mm}^3$
- Concrete -  $100 \text{ mm}^3$

## 2.3 Concept of continuum damage mechanics (CDM)

The basic concept of CDM is that a set of damage variables can represent the microstructural defects in a material. Continuum damage mechanics first represent the damage state of a material in terms of a set of internal state variables and then describe the mechanical behaviour of the damaged material and then development of damage by use of these state variables. The mechanical behaviour of a damaged material can be described using the notion of effective stress, together with the hypothesis of mechanical equivalence between damaged and undamaged material (Murakami, 2012). The concept of effective stress and mechanical equivalence will be discussed in the following sections.

### 2.3.1 Modelling by Effective area reduction

Let us consider body  $B$  of Fig. (2.2) and take an RVE at a point  $P(x)$  in  $B$ . If the total void area in  $dA$  is  $dA_D$ , the mechanical effect of  $dA$  will be decreased by  $dA_D$ . Then the area,

$$d\tilde{A} = dA - dA_D \quad (2.1)$$

may be interpreted as the area which carries the internal force and is called an *effective area* (Kachanov, 1986). Thus, the damage variable  $D$  can be specified as

$$D = \frac{dA - d\tilde{A}}{dA} = \frac{dA_D}{dA} \quad (2.2)$$

where the damage variable  $D$  takes a value between 0 and 1 ( $0 \leq D \leq 1$ ).  $D = 0$  represents initial undamaged state and  $D = 1$  represents fully damaged state.

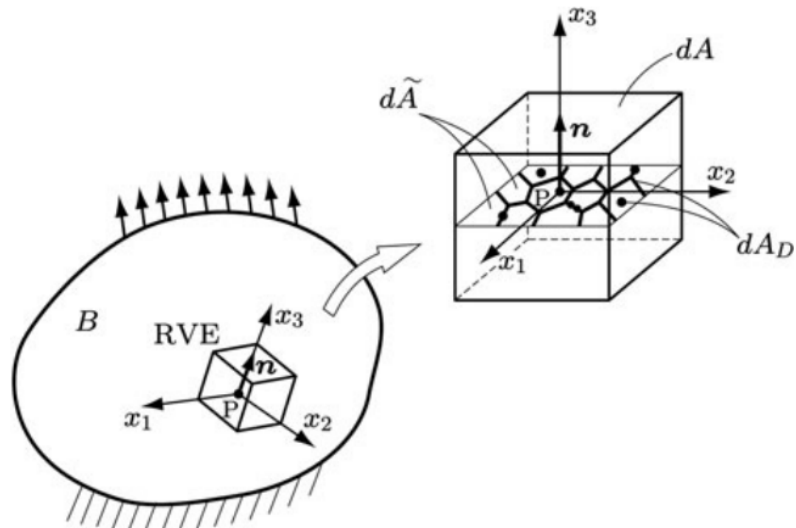


Figure 2.2: Effective area reduction due to microcracks (Murakami, 2012)

Suppose a cylindrical bar of cross-sectional area  $dA$  is subject to a tensile load  $dF$ , then the actual load carrying area is  $d\tilde{A}$  rather than  $dA$ . According to eqns (2.1) and (2.2) the effective area  $d\tilde{A}$  is given by,

$$d\tilde{A} = (1 - D)dA \quad (2.3)$$

The decrease in the load-carrying area increases the effect of stress  $\sigma$  induced by the external force  $dF$ . Due to eqn 2.3, the magnified stress  $\tilde{\sigma}$  is given by,

$$\tilde{\sigma} = \frac{dF}{d\tilde{A}} = \frac{\sigma}{1 - D} \quad (2.4)$$

Since the stress  $\tilde{\sigma}$  represents the stress magnified by the net area reduction due to damage, it is called *effective stress* (Kachanov, 1986). From eqn (2.3) and (2.4) we can postulate that the damaged cylindrical bar of Figure.(2.3b) with the cross-sectional area  $dA$  subject to force  $dF$  is mechanically equivalent to the fictitious undamaged bar of Figure.(2.3c), which is subject to force  $dF$ , has the cross-sectional area  $d\tilde{A}$  and hence stress  $\tilde{\sigma}$ . (Note - The concept and equations in this section are derived from (Murakami, 2012))

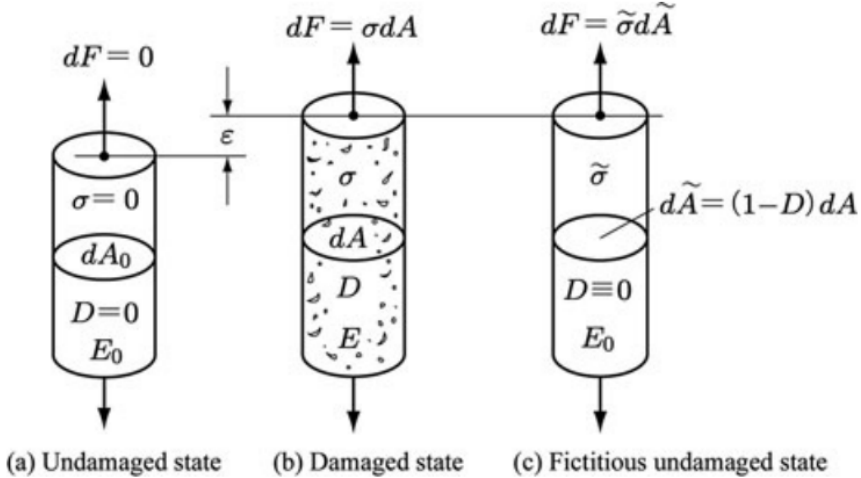


Figure 2.3: Damage of bar under tensile load (Murakami, 2012)

### 2.3.2 Modelling by variation of elastic modulus

Since the development of microcracks causes the reduction in material stiffness, the damage state can be characterized by variation in elastic modulus (Lemaitre and Chaboche, 1978). Let us consider the bar (b) and (c) of Figure. (2.3) are in the damaged and fictitious undamaged state, respectively. Then the elastic strain  $\epsilon$

in the bar (c) due to stress  $\tilde{\sigma}$  should be equal to the  $\epsilon$  of the bar (b) under stress  $\sigma$ ; i.e.,

$$\tilde{\sigma} = E_0 \epsilon, \quad \sigma = E(D) \epsilon \quad (2.5)$$

$$\epsilon = \frac{\sigma}{E(D)} = \frac{\tilde{\sigma}}{E_0} \quad (2.6)$$

where  $E_0$  and  $E(D)$  are the young's modulus of the material in the initial undamaged state and in damaged state after loading, respectively. Therefore, eqn. (2.6) defines another effective stress

$$\tilde{\sigma} = \frac{E_0}{E(D)} \sigma \quad (2.7)$$

By combining Eqn. (2.4) and (2.6) we get,

$$E(D) = (1 - D) E_0 \quad (2.8)$$

$$D = 1 - \frac{E(D)}{E_0} \quad (2.9)$$

Therefore, the damage variable  $D$  is characterized by the variation in Young's modulus  $E(D)$ . The modelling of damage by means of reduction in stiffness can be applied also to the anisotropic damage of brittle materials like composite materials, concrete, rocks etc., (Note - The concept and equations in this section are derived from (Murakami, 2012))

## 2.4 Mechanical representation of the damage state

The deformation of material depends on the direction of applied stress or strain, and hence it is an anisotropic phenomena. Therefore different theories have been developed for modelling 3-D anisotropic damage phenomenon (Murakami, 2012). Some fundamental theories that describe 3-D damage state are given below.

### 2.4.1 Scalar damage variable

In the case of random or isotropic distribution of microcracks or voids, and when void density is small, the global mechanical properties can be approximated as nearly isotropic. The damage state, in this case, may be represented using scalar damage variable  $D$ . Thus isotropic damage theory based on isotropic damage variable has been often applied to 3-D problems of creep, elastic-plastic, ductile and fatigue damage (Lemaitre, 2012)

## 2.4.2 Vector damage variable

The damage state can be specified by the decrease in load carrying effective area due to void development. Hence it is easy to postulate a vector damage variable. (Kachanov, 1986) tried to extend the definition of damage to anisotropic damage by noting a surface element in an arbitrary direction  $n$ , he proposed vector damage variable  $\omega = \omega_n n$ , where  $\omega_n$  is the effective area fraction.

## 2.4.3 Damage tensor of second order

To describe an anisotropic damage state, a damage variable of second or higher order tensor is required. Eqn.(2.3) suggests that the damage state (1 - D) is specified by the transformation of the surface element  $dA$  of Fig. (2.3b) of the damage state into the corresponding surface element  $d\tilde{A}$  in the fictitious undamaged state of Fig.(2.3c) (Murakami, 2012).

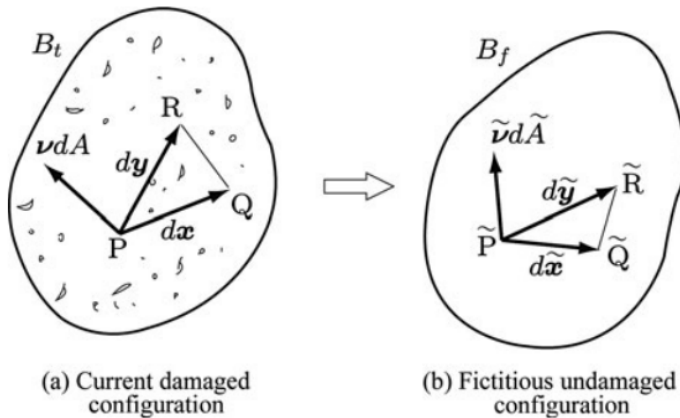


Figure 2.4: Surface element in RVE of a damaged material (Murakami, 2012)

To express damage as a second order tensor, we first consider an arbitrary surface element  $PQR$  in RVE in the current damaged configuration  $B_t$  of Fig.(2.4a). The unit normal vector and area of  $PQR$  are denoted by  $\nu$  and  $dA$ . We further postulate the fictitious undamaged configuration  $B_f$  of Fig.(2.4b) mechanically equivalent to  $B_t$ , and the surface element and its area vector are denoted by  $\tilde{P}\tilde{Q}\tilde{R}$  and  $\tilde{\nu}d\tilde{A}$  respectively. According to Eqn.(2.3) the damage variable of second-order tensor  $D$  should be defined by linear transformation from area vector  $\nu dA$  in  $B_t$  into  $\tilde{\nu}d\tilde{A}$  in  $B_f$ , i.e.,

$$\tilde{\nu}d\tilde{A} = (I - D)\nu dA \quad (2.10)$$

where  $I$  is the second order identity tensor. Since the damage tensor  $D$  is symmetric,

it can be expressed by its spectral decomposition

$$D = \sum_{i=1}^3 D_i n_i \otimes D_i n_i \quad (2.11)$$

where  $D_i$  and  $n_i$  are the principal values and principal directions of  $D$ . (Note - The concept and equations in this section are derived from (Murakami, 2012))

## 2.5 Effective Stress Tensors

The effective stresses are used to describe the mechanical behaviour of the damaged material. Some of the effective stresses postulated in damage mechanics are given below

### 2.5.1 Effective stress tensor for isotropic damage (Lemaître and Chaboche, 1978)

If the damage state is isotropic then the effective stress tensor of three-dimensional state is given by

$$\tilde{\sigma} = (1 - D)^{-1} \sigma \quad (2.12)$$

where  $D$  is the scalar damage variable, and  $\sigma$  is the Cauchy stress tensor. This effective stress simplifies damage theory and can be applied to a number of damage problems like ductile damage. But this cannot be applied to damage of significant anisotropy, such as brittle damage due to microcrack distribution.

### 2.5.2 Asymmetric effective stress tensor for anisotropic damage (Murakami, 2012)

The increase in stress caused by the net area reduction in case of anisotropic damage is given by

$$\tilde{\sigma} = (I - D)^{-1} \sigma \quad (2.13)$$

where  $I$  and  $D$  are second-order identity tensor and the second-order damage tensor, respectively. In the actual development of anisotropic damage, the stress-induced in the RVE of damage material is asymmetric. But asymmetric stress tensors make the numerical analysis complicated, and thus different methods of symmetrization have been proposed. A few of them are described as follows

### 2.5.3 Symmetrized effective stress tensor for anisotropic damage (Murakami, 2012)

A simple symmetrization procedure of Eq.(2.13) gives,

$$\tilde{\sigma} = \frac{1}{2}[(I - D)^{-1} \sigma + \sigma(I - D)^{-1}] \quad (2.14)$$

## 2.6 Damage effect tensors

The general form of an effective stress tensor  $\tilde{\sigma}$  is given by the damage effect tensor  $\mathbb{M}$  and the corresponding Cauchy stress tensor  $\sigma$ , i.e.,

$$\tilde{\sigma} = \mathbb{M} : \sigma \quad (2.15)$$

It is convenient to express the tensors in the form of matrices and then execute the tensor operations as a matrix calculus.. To simplify this procedure, we take an orthonormal basis  $n_i$  with principal directions  $n_i$  of the second-order symmetric damage tensor  $D$ , and represent the tensor in terms of its component to this basis (Murakami, 2012). According to Voigt notation, the second-order symmetric tensor  $\sigma$  and the related effective stress  $\tilde{\sigma}$  are expressed by the column vector of six dimensions:

$$[\sigma_P] \equiv [\sigma_{11} \ \sigma_{22} \ \sigma_{33} \ \sigma_{12} \ \sigma_{13} \ \sigma_{23}]^T \quad (2.16)$$

$$[\tilde{\sigma}_P] \equiv [\tilde{\sigma}_{11} \ \tilde{\sigma}_{22} \ \tilde{\sigma}_{33} \ \tilde{\sigma}_{12} \ \tilde{\sigma}_{13} \ \tilde{\sigma}_{23}]^T \quad (2.17)$$

By means of the matrix representation, we have the matrix form

$$[\tilde{\sigma}_P] \equiv [\mathbb{M}_{pq}] : [\sigma_P] \quad (2.18)$$

Matrix representation of the damage effect tensor of Eq.(2.18) is shown below (Wang et al., 2009)

$$[\mathbb{M}_{pq}] \equiv \begin{bmatrix} \frac{1}{\omega_{11}} & 0 & 0 & 0 & 0 & 0 \\ 0 & \frac{1}{\omega_{22}} & 0 & 0 & 0 & 0 \\ 0 & 0 & \frac{1}{\omega_{33}} & 0 & 0 & 0 \\ 0 & 0 & 0 & \frac{1}{\omega_{12}} & 0 & 0 \\ 0 & 0 & 0 & 0 & \frac{1}{\omega_{23}} & 0 \\ 0 & 0 & 0 & 0 & 0 & \frac{1}{\omega_{13}} \end{bmatrix}$$

where

$$\begin{aligned} \omega_{11} &= (1 - d_1); \quad \omega_{22} = (1 - d_2); \quad \omega_{33} = (1 - d_3); \\ \omega_{12} &= \sqrt{(1 - d_1)(1 - d_2)}; \quad \omega_{23} = \sqrt{(1 - d_2)(1 - d_3)}; \quad \omega_{13} = \sqrt{(1 - d_1)(1 - d_3)}; \end{aligned}$$

## 2.7 Hypothesis of strain Equivalence

The inelastic constitutive equation of a damaged material is given by the constitutive equation for an undamaged material by replacing the stress tensor  $\sigma$  in the equation with the effective stress tensor  $\tilde{\sigma}$  (Lemaitre and Chaboche, 1978). In Figure (2.5). the effect of stress  $\sigma$  acting on RVE in the current damaged configuration  $B_t$  is equivalent to that of the stress  $\tilde{\sigma}$  in the fictitious undamaged configuration. Therefore the deformation of the damaged material subject to stress  $\sigma$  should be equal to that of the fictitious undamaged material subject to stress  $\tilde{\sigma}$ . Suppose the constitutive equation of an undamaged inelastic material is given by

$$\epsilon = F_0(\sigma, \alpha) \tag{2.19}$$

or

$$\dot{\epsilon} = F_0(\sigma, \alpha) \tag{2.20}$$

where  $\alpha$  is an internal variable representing the internal change other than damage. and  $(\cdot)$  denotes the material time derivative Then according to hypothesis of strain equivalence, the inelastic constitutive equation of the damaged material represented by a damage variable  $D$  should be given by replacing  $\sigma$  of Eq.(25) with the effective stress  $\tilde{\sigma}$  i.e.,

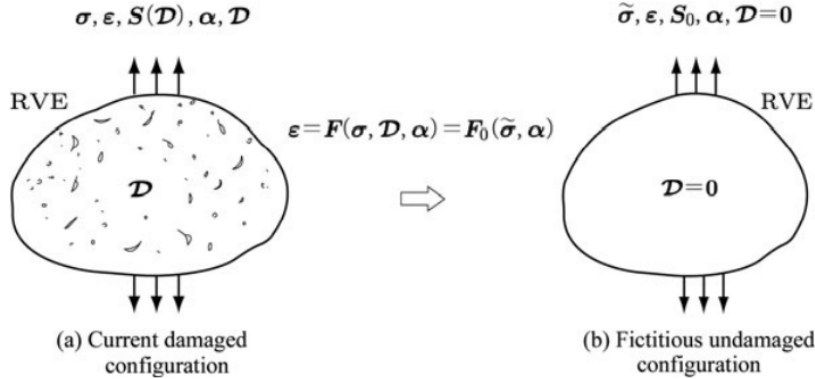


Figure 2.5: Hypothesis of strain equivalence (Murakami, 2012)

$$\epsilon = F(\sigma, D, \alpha) = F_0(\tilde{\sigma}, \alpha) \quad (2.21)$$

or

$$\dot{\epsilon} = F(\sigma, D, \alpha) = F_0(\tilde{\sigma}, \alpha) \quad (2.22)$$

In case of elastic deformation, constitutive equations for an undamaged and damaged material are given by

$$\epsilon = \mathbb{S}_0 : \sigma, \quad (2.23)$$

$$\epsilon = \mathbb{S}(D) : \sigma, \quad (2.24)$$

where  $\mathbb{S}_0$  and  $\mathbb{S}(D)$  are fourth-order elastic compliance tensors of the materials. Therefore, according to the hypothesis of strain equivalence the elastic constitutive equation of the damaged material and the compliance tensor are given by

$$\epsilon = \mathbb{S}_0 : \tilde{\sigma} = [\mathbb{S}_0 : \mathbb{M}(D)] : \sigma = \mathbb{S}(D) : \sigma \quad (2.25)$$

$$\mathbb{S}(D) = \mathbb{S}_0 : \mathbb{M}(D) \quad (2.26)$$

where  $\mathbb{M}(D)$  is the damage effect tensor which is given by

$$\mathbb{M}(D) = \mathbb{S}_0^{-1} : \mathbb{S}(D) \quad (2.27)$$

(Note - The concept and equations in this section are derived from (Murakami, 2012))

## 2.8 Hypothesis of strain energy equivalence

The existence of a strain energy function necessitates the symmetry of the compliance and elastic modulus tensor. But the compliance tensor resulting from

the hypothesis of strain equivalence is asymmetric which does not satisfy the requirement. Therefore the hypothesis of strain energy equivalence is used to satisfy the symmetry requirements (Cordebois and Sidoroff, 1982). Let us consider an elastic-plastic material and represent the plastic deformation by an internal state variable  $\alpha$ . The complementary strain energy functions of the material at undamaged and damaged state are given, respectively as follows

$$V_0(\sigma, \alpha) = \frac{1}{2}\sigma : \mathbb{S}_0 : \sigma - \phi(\alpha) \quad (2.28)$$

$$V(\sigma, D, \alpha) = \frac{1}{2}\sigma : \mathbb{S}(D) : \sigma - \phi(\alpha) \quad (2.29)$$

Thus the constitutive equation for the undamaged and damaged material is

$$\epsilon = \frac{\partial V_0}{\partial \sigma} = \mathbb{S}_0 : \sigma \quad (2.30)$$

$$\epsilon = \frac{\partial V}{\partial \sigma} = \mathbb{S}(D) : \sigma \quad (2.31)$$

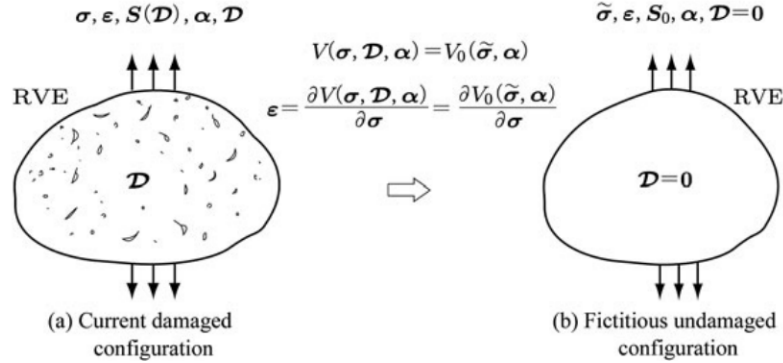


Figure 2.6: Hypothesis of strain energy equivalence (Murakami, 2012)

Suppose a damaged material of Figure.(2.6)a subject to stress  $\sigma$ , and represent the damage and internal state due to inelastic deformation by  $D$  and  $\alpha$ , respectively. Then the strain energy function  $V(\sigma, D, \alpha)$  of the damaged material is given by replacing  $\sigma$  in the corresponding function  $V_0(\sigma, \alpha)$  of the undamaged material of Fig.(2.6)b with the effective stress  $\tilde{\sigma}$

$$V(\sigma, D, \alpha) = V_0(\tilde{\sigma}, \alpha)$$

By the use of this hypothesis, the elastic strain of Eq.(2.31) leads to

$$\begin{aligned}
\epsilon &= \frac{\partial V(\sigma, D, \alpha)}{\partial \sigma} = \mathbb{S}(D) : \sigma \\
&= \frac{\partial V_0(\tilde{\sigma}, \alpha)}{\partial \sigma} = \frac{\partial}{\partial \sigma} \left( \frac{1}{2} \tilde{\sigma} : \mathbb{S}_0 : \tilde{\sigma} \right) \\
&= \frac{1}{2} \frac{\partial}{\partial \sigma} [(\mathbb{M}(D) : \sigma) : \mathbb{S}_0 : (\mathbb{M}(D) : \sigma)] \\
&= [\mathbb{M}^T(D) : \mathbb{S}_0 : \mathbb{M}(D)]
\end{aligned} \tag{2.32}$$

From Eq.(2.32), the elastic compliance tensor of the damaged material is given as follows

$$\mathbb{S}(D) = \mathbb{M}^T(D) : \mathbb{S}_0 : \mathbb{M}(D) \tag{2.33}$$

If the damage effect tensor  $\mathbb{M}(D)$  can be expressed as a fourth-order symmetric tensor, then the elastic compliance tensor  $\mathbb{S}(D)$  becomes a fourth-order symmetric tensor which satisfies the symmetry requirement. (Note - The concept and equations in this section are derived from (Murakami, 2012))

## 2.9 Elastic constitutive equation and elastic modulus tensor of orthotropic material

Orthotropic materials are materials that exhibit different material properties in the mutually perpendicular directions. They are a special form of anisotropic materials because their properties change when measured from different directions. Some examples of orthotropic materials are wood, composite materials etc., Orthotropic materials require 9 independent variables to express their constitutive matrix (efunda). The 9 elastic constants are three Young's moduli  $E_x, E_y, E_z$ , the three Poisson's ratios  $\nu_{xy}, \nu_{yz}, \nu_{zx}$ , and three shear moduli  $G_{xy}, G_{yz}, G_{zx}$ . The constitutive equation and elastic stiffness matrix of orthotropic material (Lempriere, 1968) has the form,

$$\sigma = \mathbb{C}_0 : \epsilon \quad or \quad \sigma_{ij} = C_{ijkl}^0 \epsilon_{kl}, \tag{2.34}$$

$$[C_{pq}^0] = \begin{bmatrix} \frac{1 - \nu_{yz}\nu_{zy}}{E_y E_z \Delta} & \frac{\nu_{xy} + \nu_{xz}\nu_{zy}}{E_y E_z \Delta} & \frac{\nu_{xz} + \nu_{xy}\nu_{yz}}{E_y E_z \Delta} & 0 & 0 & 0 \\ \frac{\nu_{yx} + \nu_{yz}\nu_{zx}}{E_x E_z \Delta} & \frac{1 - \nu_{xz}\nu_{zx}}{E_1 E_z \Delta} & \frac{\nu_{yz} + \nu_{yx}\nu_{xz}}{E_1 E_z \Delta} & 0 & 0 & 0 \\ \frac{\nu_{zx} + \nu_{yx}\nu_{zy}}{E_x E_y \Delta} & \frac{\nu_{zy} + \nu_{xy}\nu_{zx}}{E_x E_y \Delta} & \frac{1 - \nu_{xy}\nu_{yx}}{E_x E_y \Delta} & 0 & 0 & 0 \\ 0 & 0 & 0 & G_{xy} & 0 & 0 \\ 0 & 0 & 0 & 0 & G_{yz} & 0 \\ 0 & 0 & 0 & 0 & 0 & G_{zx} \end{bmatrix}$$

where

$$\Delta = (1 - \nu_{xy}\nu_{yx} - \nu_{yz}\nu_{zy} - \nu_{zx}\nu_{xz} - 2\nu_{xy}\nu_{yz}\nu_{zx}) / E_x E_y E_z$$

$$\text{and } \frac{\nu_{xy}}{E_y} = \frac{\nu_{yx}}{E_x}, \frac{\nu_{yz}}{E_z} = \frac{\nu_{zy}}{E_y}, \frac{\nu_{xz}}{E_z} = \frac{\nu_{zx}}{E_x}$$



# Chapter 3

## Working environment

The material models necessary for simulating progressive damage must be programmed first using a programming language, compiled, and then tested in a commercial FEM software. The programming language of choice for most commercial FEM software is FORTRAN because it is fast and straightforward. To program the material model, an integrated development environment (IDE) and a compiler compatible with the version of the FEM software are required. This chapter describes the tools required for creating damage models and instructions on how to use them in order to test the models in detail.

### 3.1 Software tools required

- **GNU Octave**

GNU Octave is software which uses a high-level programming language primarily intended for numerical computations. Initially, the damage models are developed on Octave and tested using simple loading cases like uniaxial tension with the help of constitutive driver routines before implementing them as user material routine (USERMAT) in ANSYS.

- **Microsoft Visual Studio**

Microsoft Visual Studio is the IDE used for programming the damage models as user material routines using the FORTRAN programming language.

- **Intel parallel studio**

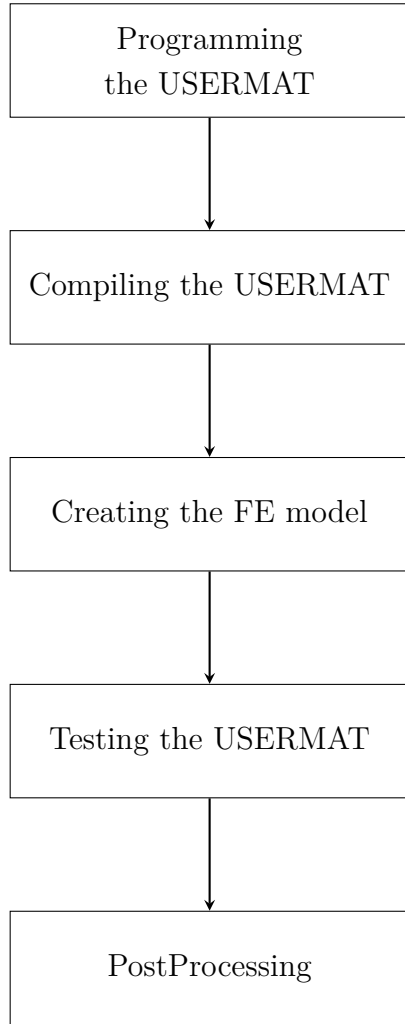
The compiler available in Intel parallel studio is used for compiling the USERMAT before testing them in a FEM software.

- **ANSYS**

ANSYS is the commercial FEM software chosen for creating models

of specimens and analyzing damage models behave under different loading conditions.

The following sections provide the reader with a detailed description, starting from developing the user material routine to implementing and analysing the results in the ANSYS environment. The flowchart below shows the steps involved in the whole process



## 3.2 Programming the USERMAT

The user material routine (USERMAT) is an ANSYS programmable feature which allows users to write their own material constitutive equations within a newly developed general material framework. The subroutine is called at all material integration points of the element during the solution phase.

ANSYS demands the necessary variables declared in a certain way so that the USERMAT developed can work compatibly with ANSYS when it is called

at each integration point. The guidelines for declaring input and output arguments can be found on ANSYS' usermat guide. The following image shows the USERMAT interface with the set of possible input arguments that USERMAT can access from ANSYS

```

subroutine usermat(
& matId, elemId,kDomIntPt, kLayer, kSectPt,
& ldstep, isubst, keycut,
& nDirect, nShear, ncomp, nStatev, nProp,
& Time, dTime, Temp, dTemp,
& stress, statev, dsdePl, sedEl, sedPl, epseq,
& Strain, dStrain, epsPl, prop, coords,
& tsstif, epsZZ,
& var1, var2, var3, var4, var5,
& var6, var7, var8)

INTEGER
& matId, elemId,
& kDomIntPt, kLayer, kSectPt,
& ldstep, isubst, keycut,
& nDirect, nShear, ncomp, nStatev, nProp
DOUBLE PRECISION
& Time, dTime, Temp, dTemp,
& sedEl, sedPl, epseq, epsZZ
DOUBLE PRECISION
& stress (ncomp ), statev (nStatev),
& dsdePl (ncomp,ncomp),
& Strain (ncomp ), dStrain (ncomp ),
& epsPl (ncomp ), prop (nProp ),
& coords (3), rotateM (3,3),
& defGrad_t(3,3), defGrad(3,3),
& tsstif (2)

```

Figure 3.1: USERMAT Interface (Lin, 1999)

For every Newton raphson iteration, the USERMAT is called at every material integration point, and ANSYS passes in strains, stresses and state variables at the beginning of the time increment and the current strain increment. The USERMAT then computes and updates the necessary output arguments like stresses and state variables at the end of the increment and the material tangent stiffness matrix  $\frac{\partial \sigma}{\partial \epsilon}$ .

### 3.3 Compiling the USERMAT

The USERMAT must be compiled before testing them in ANSYS environment. The compilation process checks for errors in the source code and converts it into ANSYS executable files (.dll files). The compiler present in Intel parallel studio is suitable for this purpose. The step by step process of compiling the USERMAT is given below

- Create an empty directory and copy the USERMAT file to be compiled (.f files) into the empty directory.
- Change the name of the USERMAT file to *usermat*

- Go to "Control Panel>Search System>Edit the system environment variables >Environment variables" and click New in the user variables for the PC, which opens a window
- In that window, type ANS\_USER\_PATH as variable name and copy and paste the path to your working directory as variable value.
- Go to folder "C:\ Program Files\ ANSYS Inc\ v(version)\ ansys\ custom\ user\ win64" and copy the ANSUSERSHARED.bat file and paste it in the working directory
- Open command prompt and navigate to the working directory
- Type ANSUSERSHARED.bat and press enter. This opens the Intel compiler and asks for USERMAT file name
- Type *usermat* without extension and press Enter.
- If there is no error in the usermat file the compiler will show the message "usermatLib.dll has been successfully build."
- For ANSYS to access these .dll files, open ANSYS Mechanical APDL product launcher and in the file management section browse to the current working directory
- By clicking run, one should see the message "Note - This ANSYS version was linked by Licensee" in the Mechanical APDL output window. This indicates that ANSYS is using the shared library with the USERMAT and the developed models can now be tested

### 3.4 Creating FE model

The preprocessor section of ANSYS mechanical APDL is used to create and mesh the FE model. The ANSYS user-programmable feature can be used with 18x family elements, which include LINK180, PLANE 182, PLANE 183, SOLID 185, SOLID 186 (Lin, 1999). The type of element required for creating FE models can be chosen from the element type menu in the preprocessor section. Once the element type is chosen, the material model, and the material properties can be entered in the *Material props* section. The *Modelling* section can be utilised to create the geometry and then can be meshed using the *Meshing* option.

To use the same FE model repetitively, to test different material models with different material properties the FE model can be saved in the form of an APDL script. An APDL script is a simple text file containing the commands required to

create and solve the FE model. A simple way to create an APDL script for an FE model is to copy the log of commands automatically created in the log file during the construction of the model and pasting it to a new text file. This log file can be accessed by going to *List > Files > Logfile*. The created APDL script can then be accessed via *File > Read input from*.

### 3.5 Testing the USERMAT

To access the user material option, the TB,USER command must be included in the APDL script. The table command for USER material option is

**TB,USER,matId,NTEMPS,NPTS (Lin, 1999)**

matId - material reference number

NTEMPS - Number of temperature points

NPTS - Number of material constants at a given temperature

If state variables are used in the USERMAT, the number of state variables need to be defined in the APDL script by the command TB,STATE

**TB,STATE,matId,,NPTS (Lin, 1999)**

matId - material reference number

NPTS - Number of state variables to be used in USERMAT

A simple example for defining a user material and two state variables is given in the Figure.(3.2) below

```
!*
YOUNG = 210e3
POISSON = 0.33
T1 = 1

TB,USER,1,1,2,
TBTEMP,T1
TBDATA,,YOUNG,POISSON
TB,STATE,1,,2
```

Figure 3.2: Table (TB) commands

Before defining boundary conditions (BCs), the entities required for solving the FE model, such as time at the end of the load step, the number of substeps, the results to be stored etc., must be defined. This can be done using *Sol'n Controls*

option in the solution menu. Once the BCs are defined, the model can be solved by giving the command *SOLVE*.

### 3.6 PostProcessing

Once the simulation completes, the results can be analyzed using the 'General Postprocessor' option. The nodal and element solutions for components like stress, strain, displacement etc., can be plotted using the 'contour plot' option, found on Plot results. By default, this option plots the results at the last substep. To plot the solution at the substep of choice one must navigate to *Read results > By pick* and select the substep to be plotted. Since the postprocessor of ANSYS does not have GUI option for plotting state variables the following command must be given: *plnsol, svar, n* where *n* is the number of the state variable to be plotted. The time history of a certain variable, such as stress, reaction force, strain etc., at a node or an element can be plotted using *TimeHist Postpro* option. On clicking the *TimeHist Postpro* option a *Variable List* window opens up (See Figure. (3.3) ). To add the variables to plot, click the green add symbol on the top-left corner which opens a window with the list of variables that can be added to the *Variable List* window. Once the variables have been added, the variables can be plotted against each other or against time. Figure.(3.3) shows the *Variable List* window with X-component of force and displacement of node 3 selected and plotted against each other.

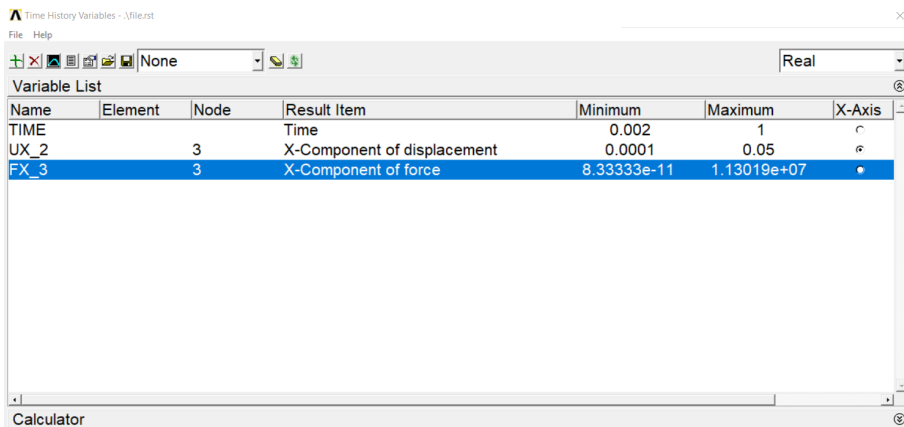


Figure 3.3: Time history post processor window

The time history results of each variable at a node or an element can also be saved as a text file using *List Data* option in the *Variable List* window.

# Chapter 4

## Progressive failure analysis of orthotropic composite materials

### 4.1 Fibre-reinforced Composites

Fibre-reinforced composites is a term for a large family of materials ranging from short fibre reinforced polyamides to unidirectional graphite fibre epoxies. They are usually orthotropic in nature i.e., their material properties differ in mutually perpendicular directions. Fibre-reinforced composites consist of three components 1) the fibres as the discontinuous or dispersed phase, 2) the matrix as the continuous phase, and 3) the fine interphase region, also known as the interface (Wikipedia). The failure in fibre reinforced composites happens mainly due to matrix cracking or fibre failure. Therefore the failure can be divided mainly into two types, namely 1) Longitudinal failure and 2) Transverse failure (Maimí et al., 2007). The mechanism of both failure in a unidirectional fibre-reinforced composite material, their causes and their effects on material behaviour are discussed in detail below

#### 4.1.1 Longitudinal failure

In fibre-reinforced plastics, the most significant portion of the load is carried by fibres. When the fibres fail, the load must redistribute to other areas of the structure and may cause structural collapse. Longitudinal tensile failure occurs as a fracture along a plane whose normal is parallel to the fibre direction. Simple maximum stress or maximum strain can usually provide an accurate measure of longitudinal tensile failure. Longitudinal compressive failure occurs from the collapse of the fibres due to shear kinking and damage of the supporting matrix. Fibre misalignment causes shear stress between fibres that rotate fibres, which increases shear stress further and leads to instability (Maimí et al., 2007).

### 4.1.2 Transverse failure

Transverse failure happens due to matrix cracking and fibre-matrix debonding. Under the presence of in-plane shear stress and transverse tensile stress, the combined effects of defects such as resin-rich regions, fibre-resin debonds etc., trigger a transverse crack that extends through the thickness. The transverse cracks are formed at the fibre-resin interface without affecting the fibres. When a unidirectional fibre composite is loaded in shear, a non-linear shear stress-strain behaviour is observed before the material fails by through-thickness matrix cracking (Maimí et al., 2007).

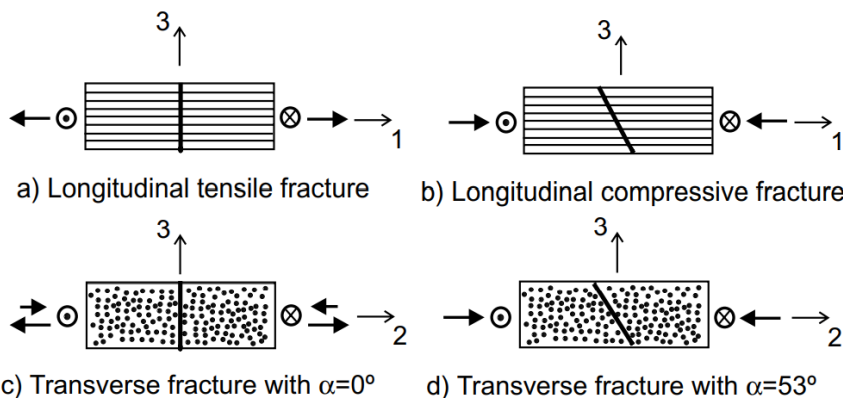


Figure 4.1: Fracture planes in FRP material (Maimí et al., 2007)

## 4.2 Damage initiation criteria

Damage initiation criteria refer to the onset of damage at a material point. Since the properties of the orthotropic composite materials are different in the mutually perpendicular directions, three failure mode indices,  $F_f$ ,  $F_m$ ,  $F_z$ , are used for failure modes in three principal material directions. Since the failure due to tension and compression in each direction cannot happen at the same integration point and at the same time, the failure mode index must be calculated based on whether the material direction is under tension or compression (Wang et al., 2009). Some of the damage initiation criteria are given as follows

### 4.2.1 3D Hashin's quadratic strain criteria

Hashin's quadratic strain criteria (Wang et al., 2009) includes shear strain components in addition to the normal strain components. The criteria for each material direction is given below

i) Longitudinal direction 1 ,

$$F_f^2 = \begin{cases} \left(\frac{\epsilon_{11}}{\epsilon_{11}^{f,t}}\right)^2 + \left(\frac{\epsilon_{12}}{\epsilon_{12}^f}\right)^2 + \left(\frac{\epsilon_{13}}{\epsilon_{13}^f}\right)^2 \geq 1 & (\epsilon_{11} > 0) \\ \left(\frac{\epsilon_{11}}{\epsilon_{11}^{f,c}}\right)^2 \geq 1 & (\epsilon_{11} < 0) \end{cases} \quad (4.1)$$

ii) Transverse direction 2,

$$F_m^2 = \begin{cases} \frac{(\epsilon_{22}+\epsilon_{33})^2}{\epsilon_{22}^{f,t}\epsilon_{33}^{f,t}} - \frac{\epsilon_{22}\epsilon_{33}}{(\epsilon_{23}^f)^2} + \left(\frac{\epsilon_{12}}{\epsilon_{12}^f}\right)^2 + \left(\frac{\epsilon_{13}}{\epsilon_{13}^f}\right)^2 + \left(\frac{\epsilon_{23}}{\epsilon_{23}^f}\right)^2 \geq 1 & (\epsilon_{22} > 0) \\ \frac{(\epsilon_{22}+\epsilon_{33})^2}{\epsilon_{22}^{f,c}\epsilon_{33}^{f,c}} + \frac{\epsilon_{22}+\epsilon_{33}}{\epsilon_{22}^{f,c}} \left( \frac{\epsilon_{22}^{f,c}}{2\epsilon_{12}^f} - 1 \right) - \frac{\epsilon_{22}\epsilon_{33}}{(\epsilon_{23}^f)^2} + \left(\frac{\epsilon_{12}}{\epsilon_{12}^f}\right)^2 \\ + \left(\frac{\epsilon_{13}}{\epsilon_{13}^f}\right)^2 + \left(\frac{\epsilon_{23}}{\epsilon_{23}^f}\right)^2 \geq 1 & (\epsilon_{22} > 0) \end{cases} \quad (4.2)$$

iii) Transverse direction 3,

$$F_z^2 = \begin{cases} \left(\frac{\epsilon_{33}}{\epsilon_{33}^{f,t}}\right)^2 + \left(\frac{\epsilon_{13}}{\epsilon_{13}^f}\right)^2 + \left(\frac{\epsilon_{23}}{\epsilon_{23}^f}\right)^2 \geq 1 & (\epsilon_{33} > 0) \\ \left(\frac{\epsilon_{33}}{\epsilon_{33}^{f,c}}\right)^2 + \left(\frac{\epsilon_{13}}{\epsilon_{13}^f}\right)^2 + \left(\frac{\epsilon_{23}}{\epsilon_{23}^f}\right)^2 \geq 1 & (\epsilon_{33} > 0) \end{cases} \quad (4.3)$$

in which  $\epsilon_{ii}^{f,t} = \frac{\sigma_i^{f,t}}{C_{ii}}$ ,  $\epsilon_{ii}^{f,c} = \frac{\sigma_i^{f,c}}{C_{ii}}$  ( $i = 1, 2, 3$ ),  $\epsilon_{12}^f = \frac{\sigma_{12}^f}{C_{44}}$ ,  $\epsilon_{13}^f = \frac{\sigma_{13}^f}{C_{55}}$ ,  $\epsilon_{23}^f = \frac{\sigma_{23}^f}{C_{66}}$

#### 4.2.2 Maximum stress criteria

Since the load-carrying area decreases due to increase in damage, the effect of stress gets magnified in the damaged material. Therefore, in the case of maximum stress criteria, normal stress components of the effective stress ( $\tilde{\sigma}$ ) are checked against the failure strength in each principal material direction. The maximum stress criteria (Jiang et al., 2018) for each material direction are given in the table below

---

Damage direction	Tension	Compression
Longitudinal direction 1 ( $F_f$ )	$\frac{\tilde{\sigma}_{11}}{X_T} \leq 1$	$\frac{\tilde{\sigma}_{11}}{-X_C} \leq 1$
Transverse direction 2 ( $F_m$ )	$\frac{\tilde{\sigma}_{22}}{Y_T} \leq 1$	$\frac{\tilde{\sigma}_{22}}{-Y_C} \leq 1$
Transverse direction 3 ( $F_z$ )	$\frac{\tilde{\sigma}_{33}}{Z_T} \leq 1$	$\frac{\tilde{\sigma}_{33}}{-Z_C} \leq 1$

---

Table 4.1: Maximum stress criterion

where  $X_T, Y_T$  and  $Z_T$  are failure strength in tension and  $X_C, Y_C$  and  $Z_C$  are failure strength in compression in each principal material direction respectively.

#### 4.2.3 Modified Hashin's failure criterion

Modified Hashin's failure criterion (Jiang et al., 2018) for plane stress condition is given below

i) Longitudinal direction 1,

$$F_f = \begin{cases} \left[ \left( \frac{\tilde{\sigma}_{11}}{X_T} \right)^2 + \alpha \cdot \left( \frac{\tilde{\sigma}_{12}}{S} \right)^2 \right]^{\frac{1}{2}} \geq 1 & (\tilde{\sigma}_{11} > 0) \\ \left[ \left( \frac{\tilde{\sigma}_{11}}{X_C} \right)^2 + \alpha \cdot \left( \frac{\tilde{\sigma}_{12}}{S} \right)^2 \right]^{\frac{1}{2}} \geq 1 & (\tilde{\sigma}_{11} < 0) \end{cases} \quad (4.4)$$

i) Transverse direction 2,

$$F_f = \begin{cases} \left[ \left( \frac{\tilde{\sigma}_{22}}{Y_T} \right)^2 + \alpha \cdot \left( \frac{\tilde{\sigma}_{12}}{S} \right)^2 \right]^{\frac{1}{2}} \geq 1 & (\tilde{\sigma}_{22} > 0) \\ \left[ \left( \frac{\tilde{\sigma}_{22}}{Y_C} \right)^2 + \alpha \cdot \left( \frac{\tilde{\sigma}_{12}}{S} \right)^2 \right]^{\frac{1}{2}} \geq 1 & (\tilde{\sigma}_{22} < 0) \end{cases} \quad (4.5)$$

where the shear contribution factor  $\alpha$  ranges from 0 to 1.

### 4.3 Types of damage evolution

Once the damage is initiated in a material point of the composite material, the stiffness must be degraded. This results in strain-softening of the composite materials rather than strain hardening, which is observed in metals. Several post-damage models have been proposed for progressive failure analysis, and most of them belong to one of the following categories (Sleight, 1999): instantaneous unloading, gradual loading, or constant stress at failure material point, as shown in Figure .(4.2)

Since continuum damage mechanics is a methodology to predict the progressive failure behaviour of composites (Wang et al., 2009), non-linear gradual unloading of the composite material is adopted and simulated in this work. Therefore non-linear material properties degradation model is implemented in this work. Based on the type of damage variable chosen, i.e., scalar, vector or second-order tensor, the damage modelling can be classified into isotropic or anisotropic damage modelling (Murakami, 2012). A brief description of the types of damage modelling, damage evolution equation used and material tangent stiffness etc. is given below

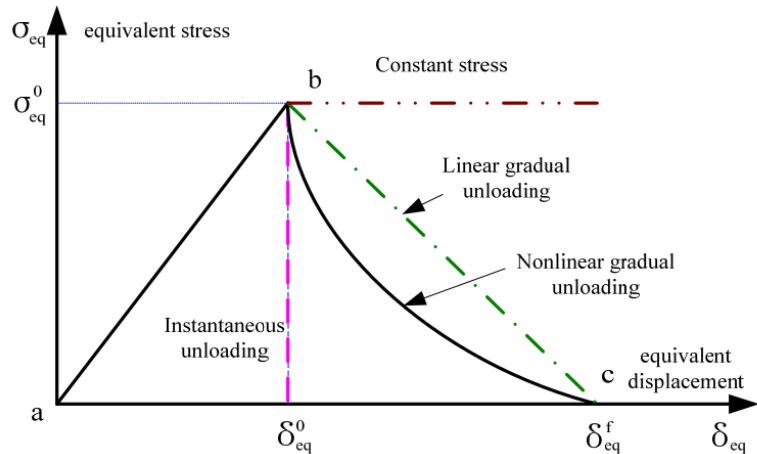


Figure 4.2: Types of degradation behaviour in damaged composite materials (Wang et al., 2009)

#### 4.3.1 Isotropic damage

In the case of isotropic distribution of cracks, the damage state is usually considered isotropic (Lemaitre, 2012), and only a scalar variable  $D$  is required to represent the damage state of the material. A simple exponential law for calculating damage evolution is given in the Eqn. (4.6) (Peerlings, 1999)

$$D = 1 - e^{-P(\tilde{\epsilon} - k)} \quad (4.6)$$

where  $P$  is the softening parameter which determines the slope of the damage evolution,  $\tilde{\epsilon}$  is the 1D equivalent strain and  $k$  is the threshold value. Since the Eqn. (4.6) is an exponential equation, the damage  $D$  evolves exponentially from 0 to 1, and the strain-softening will be an exponential decay function. Once the damage starts to evolve, the stiffness of the material must be degraded (Murakami, 2012). Therefore the elastic stiffness matrix of the damaged material is given by,

$$\mathbb{C}(D) = (1 - D)\mathbb{C}_0 \quad (4.7)$$

where  $\mathbb{C}_0$  is the material stiffness matrix of the undamaged material. Therefore the stress-strain relation for a strain softening model is given by,

$$\sigma = \mathbb{C}(D) : \epsilon \quad (4.8)$$

The finite element equations obtained for the strain-softening model are non-linear. Therefore Newton-Raphson technique is used to solve the resulting system of non-linear equations. To ensure the robustness of the Newton-Raphson method, it is important to compute the material tangent constitutive tensor  $\mathbb{C}_T$  (Lapczyk and Hurtado, 2007). It can be derived as follows,

$$\begin{aligned} \mathbb{C}_T &= \frac{\partial \sigma}{\partial \epsilon} \\ \sigma &= f(\epsilon, D) \\ \mathbb{C}_T &= \mathbb{C}(D) + \epsilon : \left( \frac{\partial \sigma}{\partial D} \otimes \frac{\partial D}{\partial \epsilon} \right) \end{aligned} \quad (4.9)$$

In the above equation, the first term  $\mathbb{C}(D)$  is the damaged elasticity matrix and second term is due increased damage. In the absence of damage propagation in an increment (For eg., during unloading), the material tangent tensor is equal to the damaged elasticity matrix, so the response is linearly elastic.

### 4.3.2 Anisotropic damage

In the case of orthotropic materials, the material property differs in the mutually perpendicular directions. Therefore it is more appropriate to choose a second-order damage tensor (Murakami, 2012). In this work, an orthotropic second-order damage tensor  $\underline{D}$  is chosen, whose principal directions are assumed to coincide with

the principal material directions. The eigenvalues of the damage tensor  $\underline{D}$  have a simple physical interpretation, i.e., the  $i^{th}$  eigenvalue  $d_i$  represents the effective fractional reduction in load carrying area on planes that are perpendicular to  $i^{th}$  principal material direction (Wang et al., 2009). The damage tensor  $\underline{D}$  can be represented as,

$$\underline{D} = \begin{bmatrix} d_1 & 0 & 0 \\ 0 & d_2 & 0 \\ 0 & 0 & d_3 \end{bmatrix}$$

A simple exponential damage evolution law (Wang et al., 2009) for each principal material direction in case of anisotropic damage is given as follows,

$$d_i = 1 - \frac{e^{-P(F_I-1)}}{F_I} \quad (4.10)$$

where  $d_i$  ( $i = 1,2,3$ ) and  $F_I$  ( $I = f,m,z$ ) are damage evolution and failure index in each principal material direction respectively. The material tangent stiffness tensor for anisotropic damage (Lapczyk and Hurtado, 2007) can also be derived in the same way as isotropic damage and it is given as follows

$$\begin{aligned} \mathbb{C}_T &= \frac{\partial \sigma}{\partial \epsilon} \\ \sigma &= f(\epsilon, \underline{D}) \\ \mathbb{C}_T &= \mathbb{C}(D) + \epsilon : \sum_{i=1}^3 \left( \frac{\partial \sigma}{\partial d_i} \otimes \frac{\partial d_i}{\partial \epsilon} \right) \end{aligned} \quad (4.11)$$

In the above equation, the first term  $\mathbb{C}(D)$  is the degraded stiffness matrix and their matrix representation for 2D/Plane-stress and 3D are given in the section () and (). In the above equation, the second term (i.e., due to increased damage) must be computed only if the corresponding failure mode is active. Since the damage evolution equation  $d_i$  depends on the failure index, the term  $\frac{\partial d_i}{\partial \epsilon}$  must be computed based on whether the corresponding damage happened during tension or compression.

## 4.4 Localisation and Mesh Regularisation

Finite element simulations which use continuum damage models are susceptible to mesh dependency. Because of the strain-softening behaviour of the material, the strain tends to localize, resulting in a strong mesh dependency, i.e., the solution is non-objective with respect to mesh refinement, and the energy dissipated decreases

with the decrease in finite element size (Lapczyk and Hurtado, 2007). Merely improving the numerical solution schemes cannot alleviate the problem associated with mesh dependency and localization. Even if the convergence to the actual solution is improved, the solution may not even make sense from a physical point of view (Peerlings, 1999). Therefore the so-called fracture energy regularization is used to reduce the mesh sensitivity. In this technique, the softening law (damage evolution law) is modified so that the amount of energy dissipated over a fully degraded finite element depends on the fracture energy of the material and the finite element size (Cervera and Chiumenti, 2006). Therefore the fracture energy ( $G_f$ ) of the material and characteristic length ( $L_c$ ) of the finite element must be included in the damage evolution equations. The damage evolution equations based on fracture energy regularization technique for each principal direction is given below (Wang et al., 2009),

In longitudinal direction 1,

$$d_1 = 1 - \frac{e^{P_1(F_f-1)}}{F_f} \quad (4.12)$$

In transverse direction 2,

$$d_2 = 1 - \frac{e^{P_2(F_m-1)}}{F_m} \quad (4.13)$$

In transverse direction 3,

$$d_3 = 1 - \frac{e^{P_3(F_z-1)}}{F_z} \quad (4.14)$$

where  $P_1 = \frac{-\sigma_{11}^f \epsilon_{11}^f L_c}{G_{f,1}}$ ,  $P_2 = \frac{-\sigma_{22}^f \epsilon_{22}^f L_c}{G_{f,2}}$  and  $P_3 = \frac{-\sigma_{33}^f \epsilon_{33}^f L_c}{G_{f,3}}$

$G_{f,i}$  - is the fracture energy in each principal direction ( $i = 1,2,3$ )

$\sigma_{ii}^f$  - failure strength in each principal direction ( $i = 1,2,3$ )

$\epsilon_{ii}^f$  - failure strain in each principal direction ( $i = 1,2,3$ )

$L_c$  - Characteristic length

## 4.5 Numerical implementation of the damage model in ANSYS

As discussed before, the material models necessary for simulating progressive damage failure are implemented using the ANSYS user-programmable feature

called USERMAT. The damage model implemented using USERMAT computes and updates the current stress and consistent tangent stiffness. The following sections deal with the numerical implementation of the damage model based on two different methods or criteria used to predict the damage initiation.

- Strain based damage model
- Stress based damage model

#### 4.5.1 Strain based damage model

In the case of the strain-based damage model, the damage initiation is predicted using current strain ( $\underline{\epsilon}_{n+1}$ ) (Wang et al., 2009). The USERMAT receives strains, stresses and state variables at the beginning of the time increment and the current strain increment. The following steps describe the process of implementing the damage model

- Calculate current strain

$$\underline{\epsilon}_{n+1} = \underline{\epsilon}_n + \Delta\epsilon$$

- Calculate the current degraded material stiffness matrix  $\mathbb{C}(\underline{D}_n)$
- Calculate the failure indices  $F_I(\underline{\epsilon})$  ( Refer to Sections (??) and (??) )

Check if  $F_I \geq F_{I\max}$

- if  $F_I(\underline{\epsilon}) < 1$

$$\underline{\sigma}_{n+1} = \mathbb{C}(\underline{D}_n) : \underline{\epsilon}_{n+1}$$

$$\mathbb{C}_T = \mathbb{C}(\underline{D}_n)$$

- else

Calculate the damage variables using damage evolution law, ( Refer to eqn (4.12) to (4.14) )

$$d_1(F_f), d_2(F_m), d_3(F_z)$$

Check if  $d_i \geq 0$

Calculate the updated degraded stiffness based on damage variables

$$\mathbb{C}(\underline{D}_{n+1})$$

Calculate current stress

$$\underline{\sigma}_{n+1} = \mathbb{C}(\underline{D}_{n+1}) : \underline{\epsilon}_{n+1}$$

Calculate tangent stiffness

$$\mathbb{C}_T = \mathbb{C}(D) + \sum_{i=1}^3 \left( \frac{\partial \mathbb{C}(D)}{\partial d_i} : \epsilon \otimes \frac{\partial d_i}{\partial \epsilon} \right)$$

#### 4.5.2 Stress based damage model

In the case of stress-based damage model, the damage initiation is predicted using effective stress ( $\tilde{\sigma}_{n+1}$ ) (Jiang et al., 2018). The USERMAT receives strains, stresses and state variables at the beginning of the time increment and the current strain increment. The following steps describe the process of implementing the damage model.

- Calculate the elastic stiffness matrix  $\mathbb{C}$
- Calculate effective stress

$$\tilde{\sigma}_{n+1} = \mathbb{C}_0 : \underline{\epsilon}_{n+1}$$

- Calculate the failure indices  $F_I(\underline{\sigma})$ , ( Refer to Section (4.2.2) and (4.2.3) )

Check if  $F_I \geq F_{I\max}$

- if  $F_I(\underline{\sigma}) < 1$

$$\underline{\sigma}_{n+1} = \tilde{\sigma}_{n+1}$$

$$\mathbb{C}_T = \mathbb{C}$$

- else

Calculate the damage variables using damage evolution law, ( Refer eqn (4.12) to (4.14) )

$$d_1(F_f), d_2(F_m), d_3(F_z)$$

Check if  $d_i \geq 0$

Calculate the updated degraded stiffness based on damage variables

$$\mathbb{C}(\underline{D}_{n+1})$$

Calculate current stress

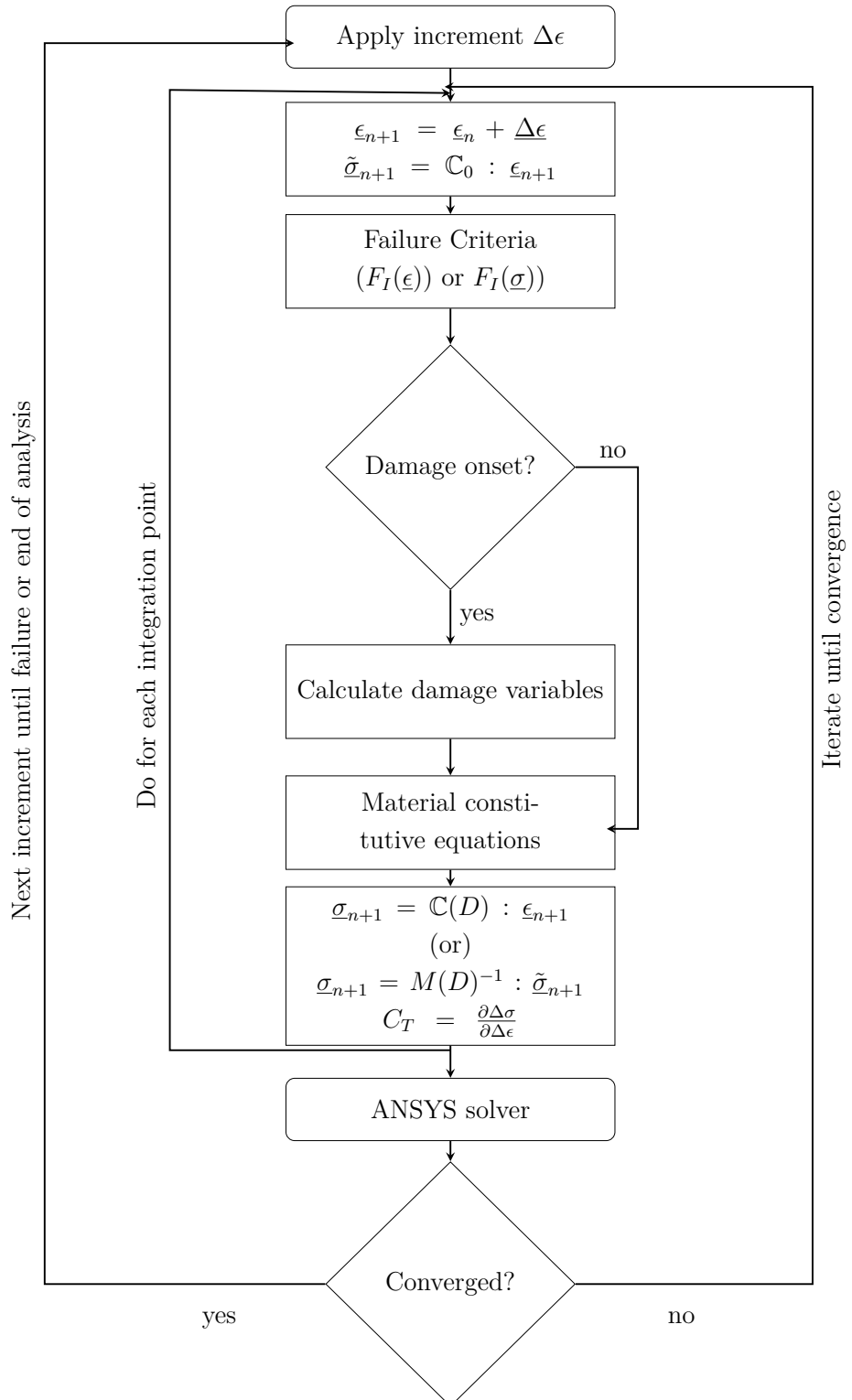
$$\underline{\sigma}_{n+1} = M(D)^{-1} : \tilde{\sigma}_{n+1}$$

Calculate tangent stiffness

$$\mathbb{C}_T = \mathbb{C}(D) + \sum_{i=1}^3 \left( \frac{\partial \mathbb{C}(D)}{\partial d_i} : \epsilon \otimes \frac{\partial d_i}{\partial \epsilon} \right)$$

## 4.6 Schematic of UMAT implementation

The flowchart below shows the schematic of the user material subroutine (USERMATERIAL) implementation for both and strain and stress based damage model and how the subroutine interacts with the ANSYS environment.





# Chapter 5

## Results and Discussion

### 5.1 Modelling linear elastic behaviour of orthotropic materials

Before implementing the damage behaviour in orthotropic materials, their linear elastic behaviour must be implemented which describes what happens before the damage initiation. As mentioned before orthotropic materials are a special class of material whose properties differ in mutually perpendicular directions. Therefore 9 independent material constants are required to model their elastic behaviour. Table (5.1) summarises the utilised material parameters. The material parameters presented in table (5.1) belongs to an unidirectional glass fiber-reinforced epoxy material obtained from (Lapczyk and Hurtado, 2007). In this material, the strength in the longitudinal direction ( $X_t$  and  $X_c$ ) is very high compared to the transverse directions ( $Y_t$  and  $Y_c$ ) because the fibers are aligned parallel to the longitudinal direction.

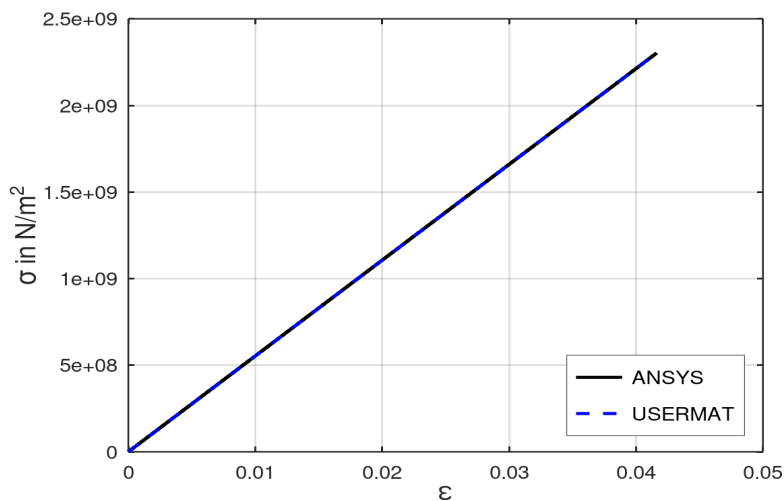


Figure 5.1: Stress-Strain relation (Standard vs user-defined material routine)

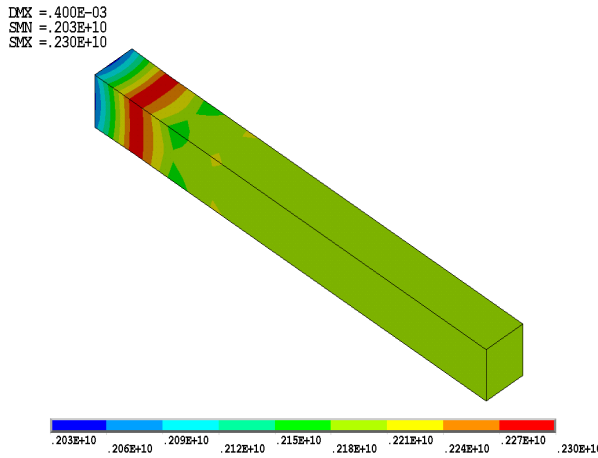
---

<b>Symbol</b>	<b>Material Parameter</b>	<b>Value</b>
$E_1$	Elastic modulus in longitudinal (1) direction	55000e6 $N/m^2$
$E_2 = E_3$	Elastic modulus in transverse (2 and 3) directions	9500e6 $N/m^2$
$\nu_{12} = \nu_{13}$	Poisson's ratio (in-plane)	0.33
$\nu_{23}$	Poisson's ratio (Planes 2-3)	0.27
$G_{12} = G_{13}$	In-plane shear modulus	5500e6 $N/m^2$
$G_{23}$	Shear modulus (Planes 2-3)	3000e6 $N/m^2$
$X_t$	Tensile strength in longitudinal (1) direction	2500e6 $N/m^2$
$X_c$	Compressive strength in longitudinal (1) direction	-2000e6 $N/m^2$
$Y_t$	Tensile strength in transverse (2 and 3) directions	50e6 $N/m^2$
$Y_c$	Compressive strength in transverse (2 and 3) directions	-200e6 $N/m^2$
$S_{12}$	In-plane strength	50e6 $N/m^2$

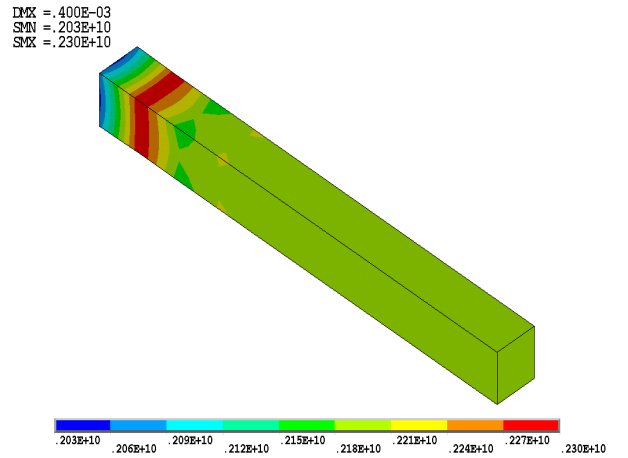
---

Table 5.1: Material parameters (Integration point studies)

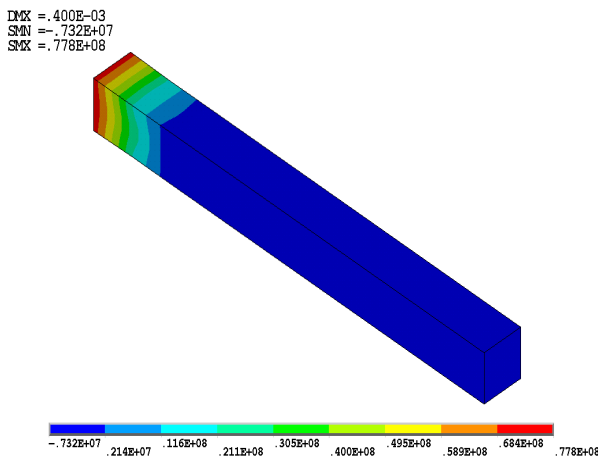
The constitutive matrix given in the section (2.9) and Hooke's law help us model the elastic behaviour of the orthotropic materials. The linear elastic behaviour of the orthotropic material is implemented as USERMAT in ANSYS, and in this section, the results obtained are compared against the standard orthotropic material routine present in ANSYS using a structural example. A bar of length 10 mm and area 1  $mm^2$  ( $b = 1\text{ mm}$ ,  $t = 1\text{ mm}$ ) fixed at one end is chosen for the analysis. The bar is constructed using 8 node SOLID 185 elements, and full integration has been used. A displacement of 1 mm is applied at the free end, and the results obtained using the standard and the user-defined material routines are presented below. Figure (5.1) compares the stress-strain relation between standard material routine and the implemented USERMAT



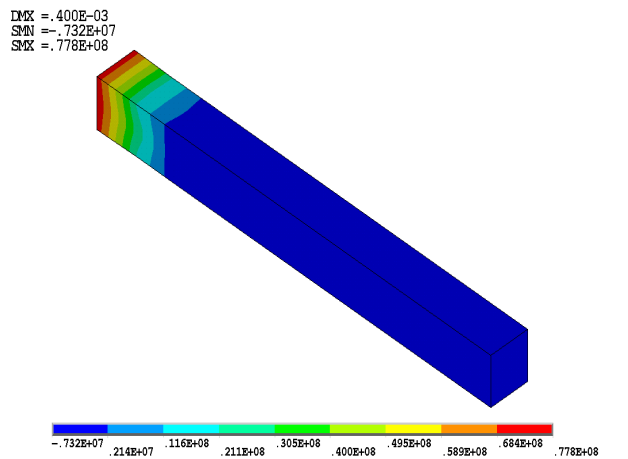
(a)  $\sigma_{11}$  Component of Stress



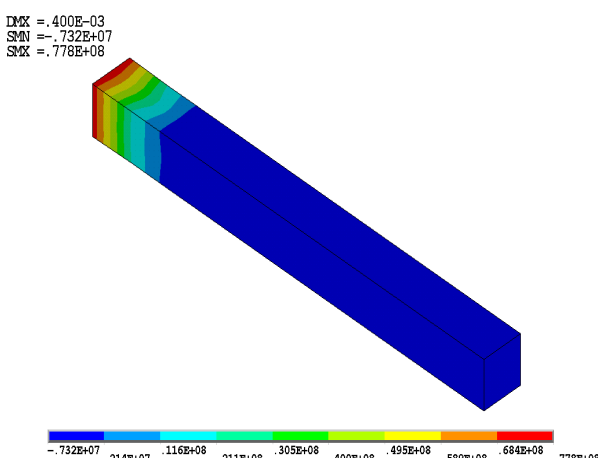
(b)  $\sigma_{11}$  Component of Stress



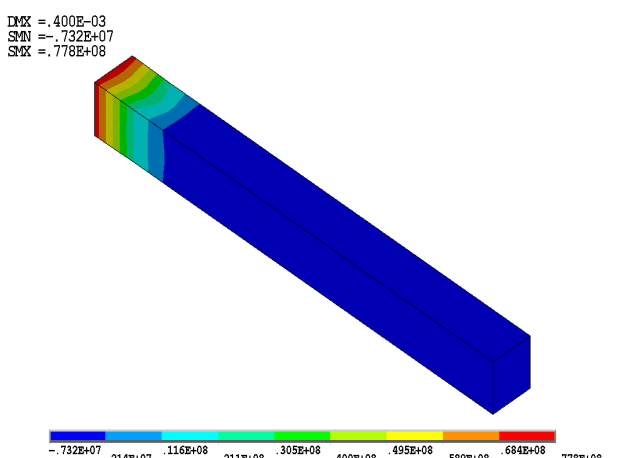
(c)  $\sigma_{22}$  Component of Stress



(d)  $\sigma_{22}$  Component of Stress



(e)  $\sigma_{33}$  Component of Stress



(f)  $\sigma_{33}$  Component of Stress

Figure 5.2: Contour plots of the stress components  $\sigma_{11}$ ,  $\sigma_{22}$  and  $\sigma_{33}$  of the bar obtained using standard (Figures a,c,e on the left) and user-defined material routine (Figures b, d, f on the right)

Figure (5.2) shows the contour plots of the normal stresses ( $\sigma_{11}$ ,  $\sigma_{22}$  and  $\sigma_{33}$ ) computed using standard and user-defined material routine respectively. The comparison of the stress-strain relation and contour plots between the both the routines confirm that the results obtained are similar and therefore further damage-initiation and damage-evolution processes can now be implemented.

## 5.2 Damage behaviour at integration point level

The material subroutines are first developed on the octave and tested using constitutive driver routines (B.Kiefer), enabling us to understand the phenomenon at the integration point level. To demonstrate the evolution of damage after damage initiation and the strain-softening, following simple loading cases are investigated at the integration point level.

- Uniaxial tension
- Biaxial tension
- Triaxial tension.

After that, the material subroutines are implemented in USERMAT and tested in the ANSYS environment using a 3D finite element of unit length. The finite element is subjected to the above loading cases, and the results are compared against the octave implementation

### 5.2.1 Uniaxial tension

In the case of uniaxial tension, the normal stress is present only in one direction, and two other normal stresses and all the shear stresses are zero, i.e., only one non-zero component is located on the main diagonal of the stress tensor (Brainkart). In the ANSYS environment, uniaxial tension is achieved by applying a displacement on the finite element in a normal direction (1), which increases the strain  $\epsilon_{11}$  linearly, and the lateral (transverse) contraction is not constrained. 3D Hashin's quadratic strain criteria (Section(4.2.1)) are used to predict the damage initiation, and the exponential damage evolution law (Eqn.4.10) is used to calculate the damage evolution. The results obtained from ANSYS and USERMAT are presented in Figure (5.3a) and (5.3b) respectively. Figure (5.4) shows the evolution of damage variables.

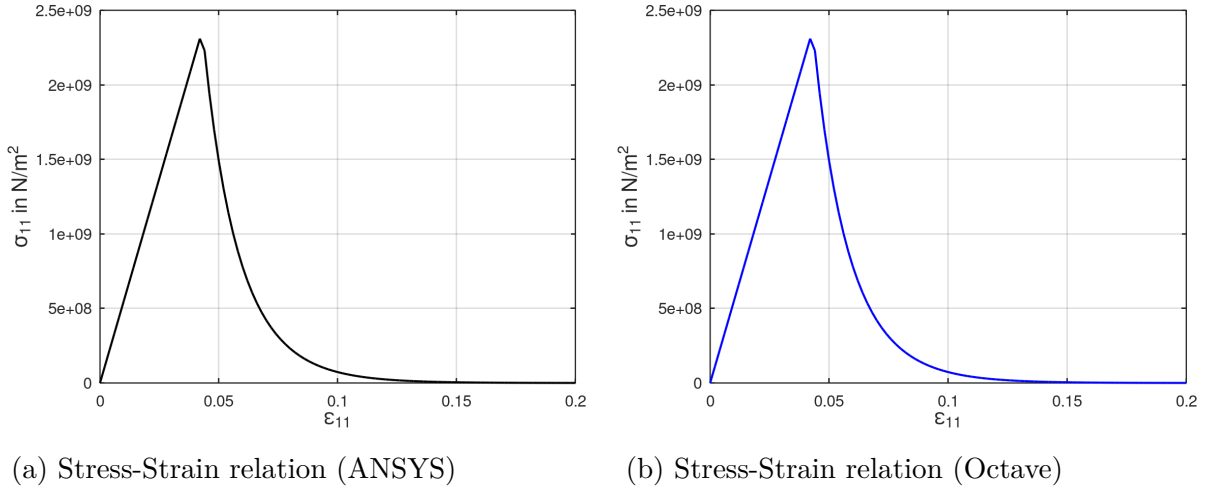


Figure 5.3: Evolution of stress for uniaxial tension test in 11 direction

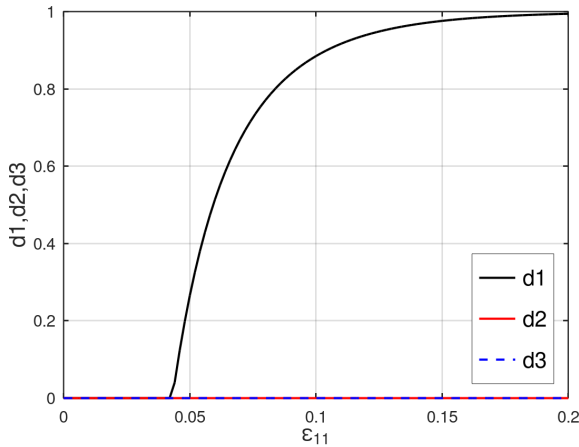


Figure 5.4: Evolution of damage components for uniaxial tension test in 11 direction

The system is linearly elastic until the damage initiation strain, and the damage is zero. Once the strain  $\epsilon_{11}$  exceeds the damage initiation strain, the damage  $d_1$  starts to evolve exponentially, and the stress starts to drop due to the reduction in stiffness in 1 direction. The damage variables  $d_2$  and  $d_3$  are zero. The comparison between the figures (5.3a) and (5.3b) suggests that the material routine implemented in octave and USERMAT are numerically similar to each other. The scalar softening parameter ( $P$ ) in the damage evolution equation(4.10) determines the slope of the damage curve. The following figure demonstrates the influence of the softening parameter ( $P$ ) on the damage evolution

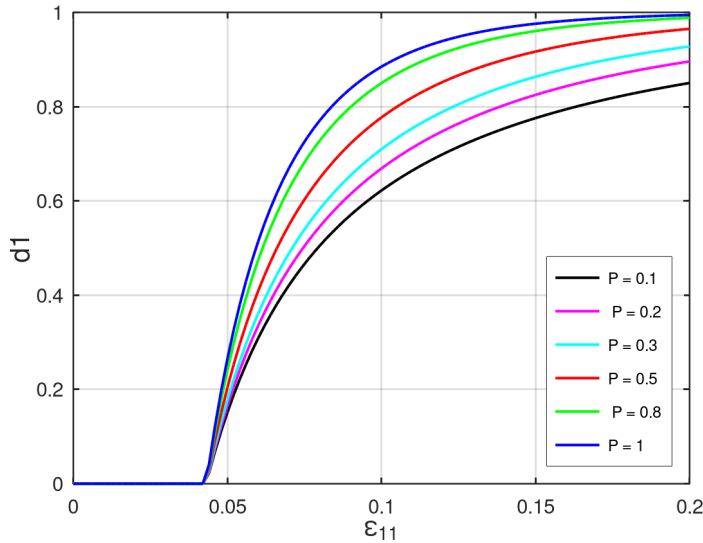


Figure 5.5: Influence of softening parameter  $P$  in the damage evolution)

#### Drawbacks of strain based damage initiation criteria

Since the lateral contraction is not constrained during uniaxial tension, the transverse directions experience negative strain due to Poisson's effect, i.e.,  $\epsilon_{22}$  and  $\epsilon_{33}$  will be negative. If the compressive strength in the transverse directions 2 and 3 are sufficiently low, the strains  $\epsilon_{22}$  and  $\epsilon_{33}$  will exceed the damage initiation strain. This leads to damage evolution without the presence of stress in transverse directions 2 and 3. This phenomenon cause convergence issues and the computation stops when the damage evolves without the presence of stress. Figure (5.6) shows the norm of the residual stress, which does not reach zero (or a below a tolerance ) after 100 iterations of the Newton-raphson, which indicates the failure of the model to converge to a solution when using low compressive strength in the transverse direction ( $Y_c = -180\text{MPa}$ )

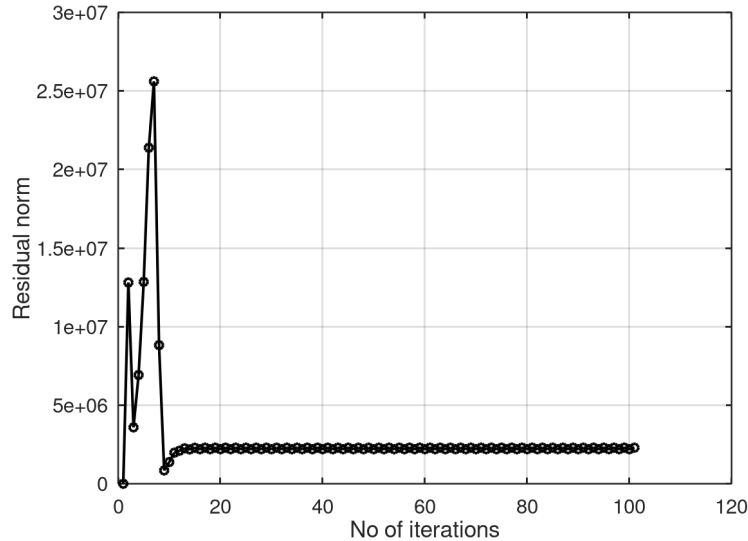


Figure 5.6: Convergence issue: Residual norm of the stress *vs* No of Newton-raphson iterations

This problem can be rectified by using stress-based damage initiation criteria. Since damage evolution depends on failure index  $F$ , the transverse failure indices  $F_m$  and  $F_z$  will be zero during uniaxial tension if the stress-based damage initiation criteria are used. This results in zero damage in the transverse direction. The following section presents the results obtained using stress-based damage initiation and the use of mesh regularisation in the damage evolution law.

#### **Stress based damage initiation and mesh regularisation**

As mentioned in section (4.4), the strain localisation problems result in strong mesh dependency, so fracture energy and characteristic length ( $L_c$ ) of the element have been included in the damage evolution law in order to alleviate the problem. So the material routine is modified by changing the damage initiation criteria to maximum stress criteria (4.1) and including the damage evolution equations from (4.12) to (4.14). The uniaxial tension is conducted again with the changes mentioned above and with very low transverse compression strength, and the results are presented below.

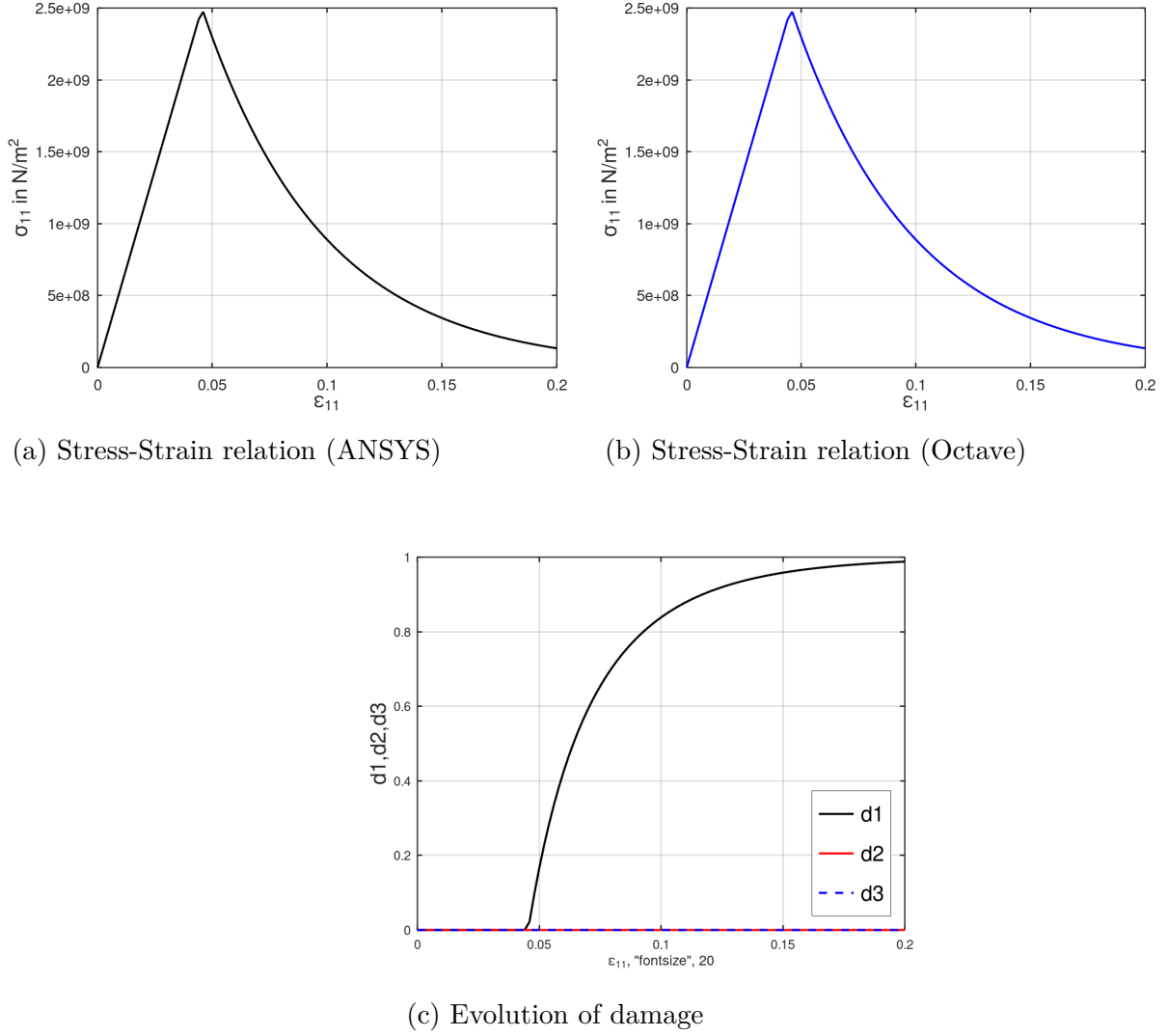


Figure 5.7: Evolution of stress and damage components with stress-based damage initiation criteria under uniaxial tension

From figure (5.7c) it is evident that the damage  $d_2$  and  $d_3$  are zero as a result of stress-based damage initiation because the stress components  $\sigma_{22}$  and  $\sigma_{33}$  are zero under uniaxial tension. While using mesh regularisation, the slope of the damage curve is determined by the characteristic length ( $L_c$ ), which depends on the volume of the element. The following figure (5.5) shows how the damage evolution is affected by the volume of the element,

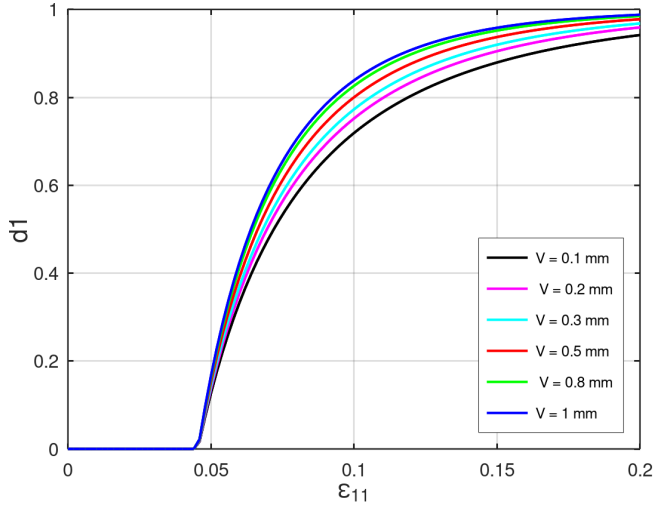


Figure 5.8: Influence of element volume ( $V$ ) on the damage evolution

### Discussion of tangent stiffness

In the case of uniaxial tension, the components of the stress tensor other than  $\sigma_{11}$  are zero. Since stress conditions are enforced, the octave driver routine (B.Kiefer) uses the Newton-raphson method to determine the input strain components other than  $\epsilon_{11}$  iteratively. The Newton-raphson method requires a tangent stiffness for computation which can be derived using the equation (4.11) for anisotropic damage. This enables us to test the derived algorithmic tangent stiffness (ATS) before implementing as USERMAT in ANSYS. The derived algorithmic tangent stiffness is verified by comparing it with the numerical tangent stiffness computed using numerical perturbation. In numerical perturbation, the coefficients of the strain tensor are perturbed by a very small value, i.e.,  $\Delta\epsilon_{kl}^{n+1} = \delta$  (where  $\delta \ll 1$ ) and the resulting stress perturbations are calculated.

$$\Delta\sigma_{ij}^{n+1} = \sigma_{ij}^{n+1}(\epsilon_{kl}^{n+1} + \delta) - \sigma_{ij}^{n+1}(\epsilon_{kl}^{n+1}) \quad (5.1)$$

Then the components of the tangent stiffness tensor can be estimated as

$$C_T = \frac{\Delta\sigma_{ij}^{n+1}}{\Delta\epsilon_{kl}^{n+1}} \quad (5.2)$$

Since the material routine must be evaluated for every perturbation of  $\epsilon_{kl}$  the routine has to be called six time recursively per load-step iteration. The figure (5.9a) and (5.9b) shows the strain components  $\epsilon_{22}$  and  $\epsilon_{33}$  computed using algorithmic and numerical tangent stiffness which are plotted against  $\epsilon_{11}$  respectively.

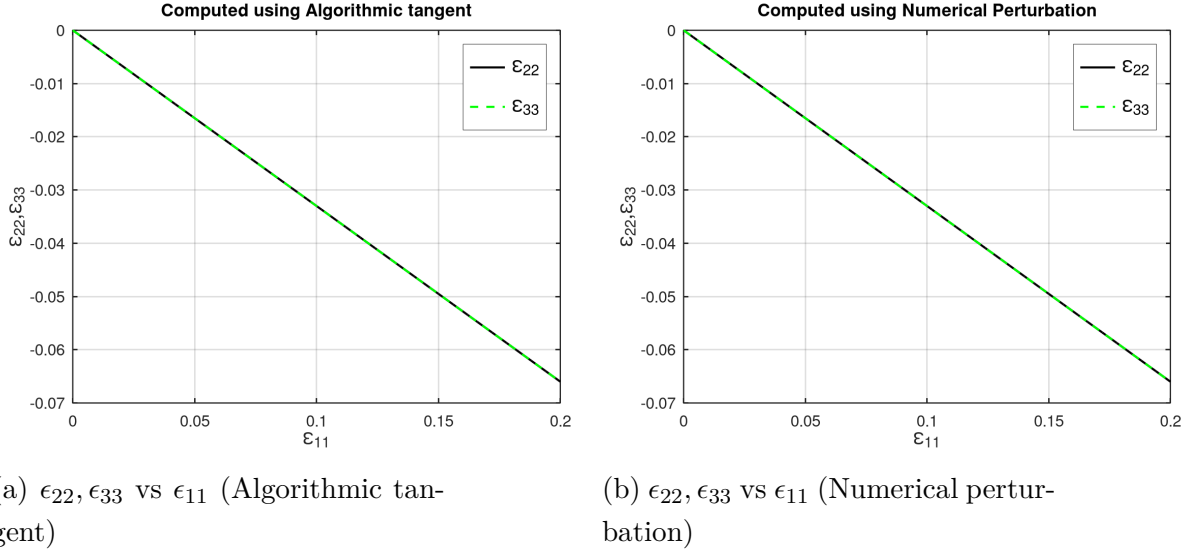


Figure 5.9: The strain components  $\epsilon_{22}$  and  $\epsilon_{33}$  computed using algorithmic (a) and numerical tangent stiffness (b) under uniaxial tension

These comparison between above plots clearly indicates that the tangent stiffness computed using algorithmic tangent and numerical tangent are numerically similar to each other.

### 5.2.2 Biaxial tension

In the case of biaxial tension, normal stresses are present only in two normal directions, and all the shear stresses are zero as well as the normal stress in third direction, i.e., only two non-zero components presented located on the main diagonal of the stress tensor (Brainkart). In ANSYS, biaxial tension is achieved by applying the same displacements in two normal directions of the finite element (1 and 2 direction), and the contraction in the third direction (3) is unconstrained. The following figures show the corresponding stress and damage components obtained from the test.

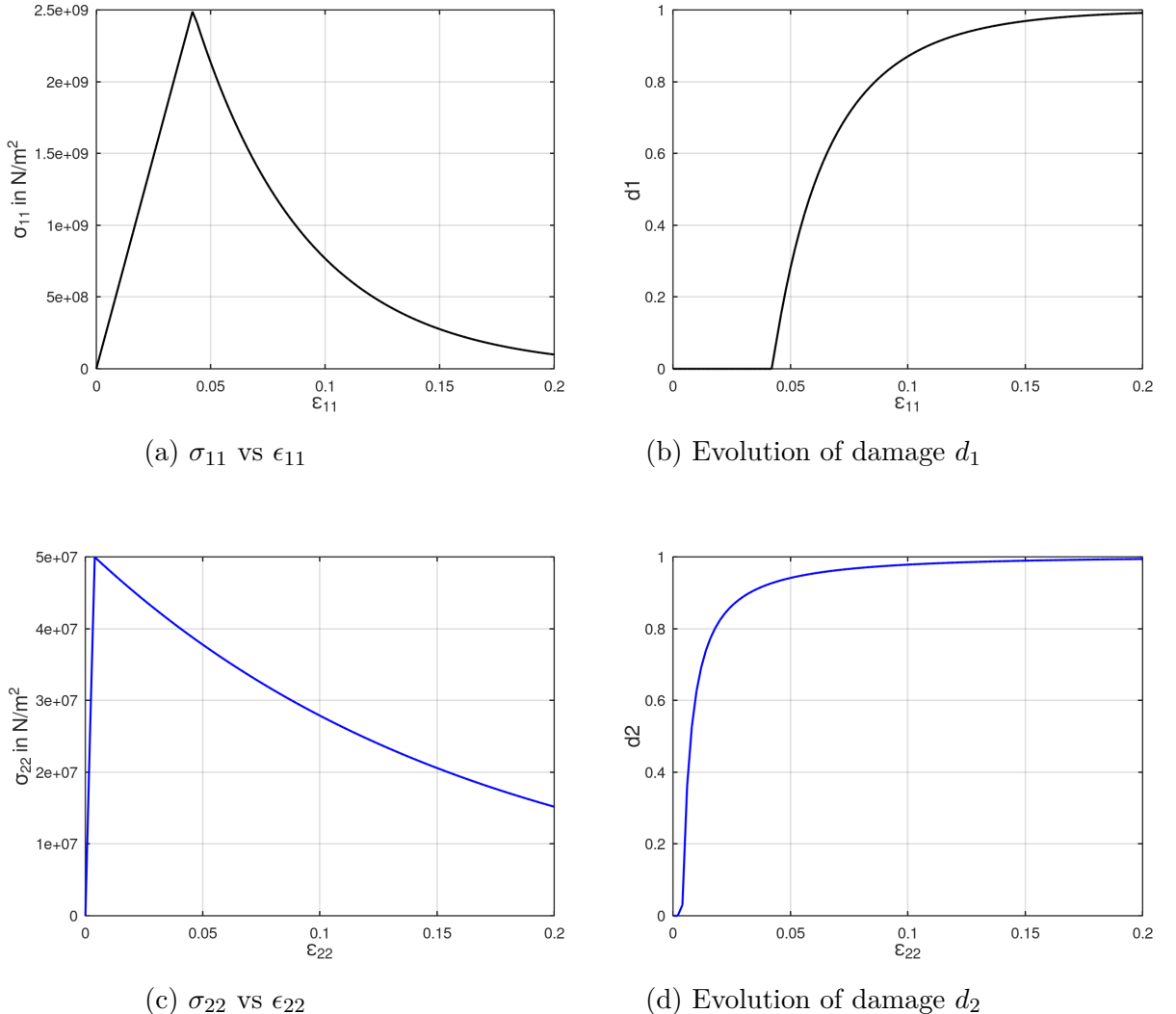
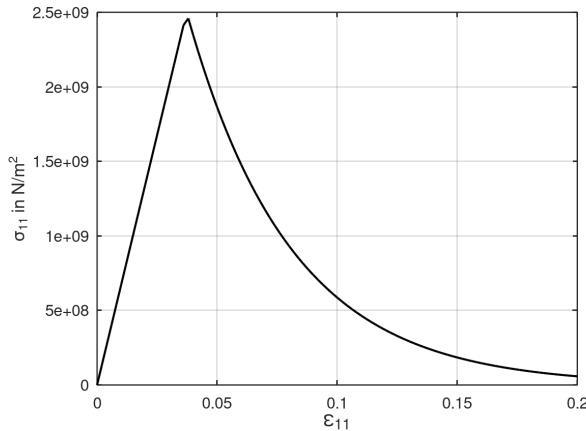


Figure 5.10: Evolution of stress (Figures a, c on the left) and corresponding damage (Figure b, d on the right) components under biaxial tension

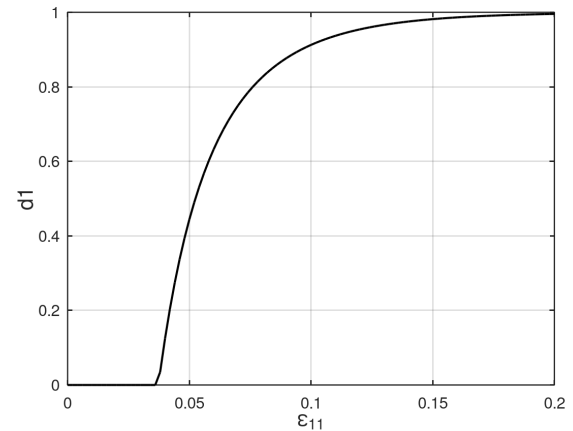
Since the tensile strength in transverse direction is very low compared to the longitudinal direction, evolution of damage ( $d_2$ ) begins very soon and simultaneously the stress component ( $\sigma_{22}$ ) drops as seen in figures (5.10c) and (5.10d).

### 5.2.3 Triaxial tension

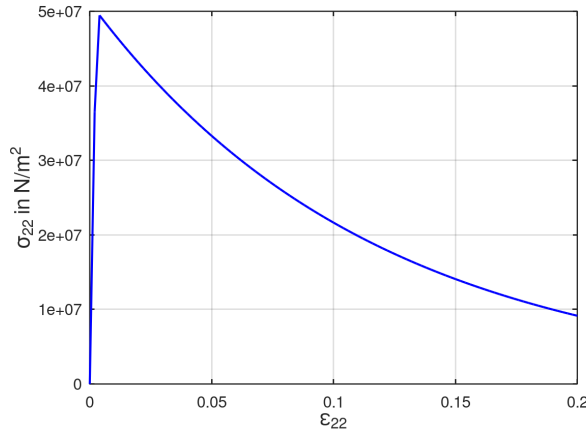
In the case of triaxial tension, the normal stresses are present in all three normal directions, and all the shear stresses are zero, i.e., only diagonal components of the stress tensor are non-zero. In Ansys, triaxial tension is achieved by applying the same displacement in all three normal directions (1, 2 and 3 direction) (Brainkart). The following figures show the corresponding stress and damage components obtained from the test.



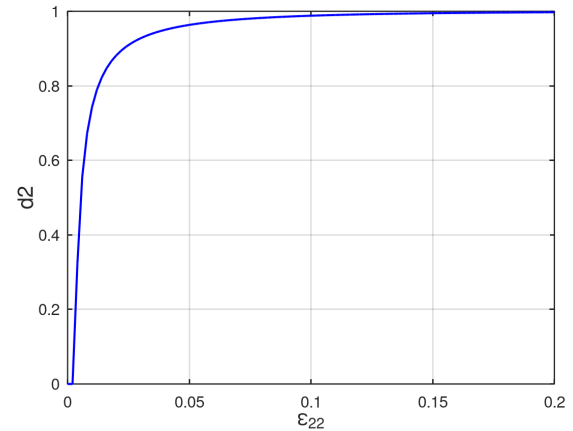
(a)  $\sigma_{11}$  vs  $\epsilon_{11}$



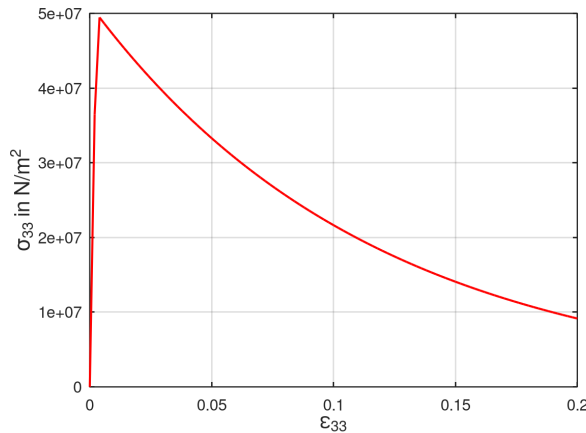
(b) Evolution of damage  $d_1$



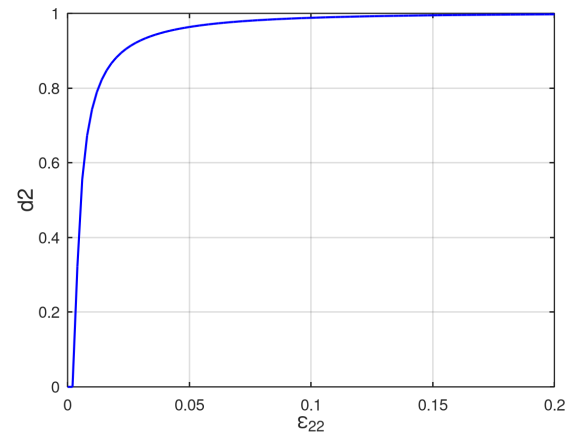
(c)  $\sigma_{22}$  vs  $\epsilon_{22}$



(d) Evolution of damage  $d_2$



(e)  $\sigma_{33}$  vs  $\epsilon_{33}$



(f) Evolution of damage  $d_3$

Figure 5.11: Evolution of stress (Figures a, c, e on the left) and corresponding (Figures b, d, f on the right) damage components under triaxial tension

Since the material properties are the same in transverse 2 and 3 direction and the

tensile strength is very low compared to the longitudinal 1 direction, the damage  $d_2$  and  $d_3$  evolves simultaneously (Figure (5.11d) and (5.11f)) and very soon as expected. Therefore the stress components  $\sigma_{22}$  and  $\sigma_{33}$  drop very soon as shown in Figure (5.11c) and (5.11e)

### 5.3 Representative structural examples

The following structural examples are used to test the damage model implemented as a USERMAT in the ANSYS environment

- Notched tensile specimen (2D - Plane stress)
- Compact tension (CT) specimen (2D - Plane stress)
- Plate with hole (3D)

Each example is chosen to demonstrate specific features of the damage model. These features include, at first, the capability of the model to represent damage initiation and propagation and secondly, the calculation of multiple damage variables, i.e., the ability to show anisotropic damage development in the composite material when a load is applied, both in 2D and 3D setting. Furthermore, mesh convergence studies are performed to show that the regularization scheme employed gives better results than the model with no regularization. For all the finite element simulations of the above models, linear quadrilateral elements are used (both 2D and 3D) with full Gauss integration. The line search option has been enabled during all the simulations to get good convergence behaviour. The material used for the finite element simulations is T700/2510 carbon fiber/epoxy fabric. The material has fibers in parallel in the longitudinal direction and fibers woven in the cross-section that provide additional strength in transverse directions. The material has a high modulus and strength in the longitudinal direction compared to the transverse direction. The material properties are obtained from (Jiang et al., 2018) and a summary of the material properties are given in the Table (5.2).

Symbol	Material Parameter	Value
$E_{11}$	Modulus in longitudinal (1) direction	55.8 GPa
$E_{22} = E_{33}$	Modulus in transverse (2 and 3) directions	54.9 GPa
$\nu_{12}$	Poisson's ratio	0.043
$G_{12} = G_{23} = G_{13}$	Shear modulus	4.2 GPa
$X_t$	Tensile strength in longitudinal (1) direction	910.1 MPa
$X_c$	Compressive strength in longitudinal (1) direction	-710.2 MPa
$Y_t$	Tensile strength in (2 and 3) directions	772.2 MPa
$Y_c$	Compressive strength in (2 and 3) directions	-703.3 MPa
$S_{12}$	In-plane strength	131 MPa
$G_f^{lt}$	Tensile fracture energy along longitudinal (1) direction	125 KJ/m <sup>2</sup>
$G_f^{lc}$	Compressive fracture energy along longitudinal (1) direction	250 KJ/m <sup>2</sup>
$G_f^{tt}$	Tensile fracture energy along (2 and 3) directions	95 KJ/m <sup>2</sup>
$G_f^{tc}$	Compressive fracture energy along (2 and 3) directions	254 KJ/m <sup>2</sup>

Table 5.2: Material parameters (Representative structural examples)

### 5.3.1 Notched tensile specimen

The first example demonstrates the model's capability to represent damage initiation and propagation. A notched tensile specimen is widely used for analysis of stress concentration, fatigue etc., Because of the symmetry, only one-quarter of the specimen is modelled in the finite element analysis and the geometry and boundary conditions are shown in the Figure (5.12). The meshes consist of plane-stress elements (PLANE 182) with bilinear interpolations for displacements, and  $2 \times 2$  Gauss integration has been utilized. Three different finite element meshes have been used in the fracture zone with the elements of  $h=1$  mm,  $0.5$  mm,  $0.25$  mm and a total of 500, 840, 1460 elements respectively for the convergence studies (Figure 5.13). At first, the longitudinal direction is kept parallel to the loading direction, and the behaviour of the model is analyzed by applying a displacement controlled load ( $U_x$ ) in the longitudinal direction (X-direction). The maximum stress criterion (Section 4.2.2) has been used to predict the damage initiation.

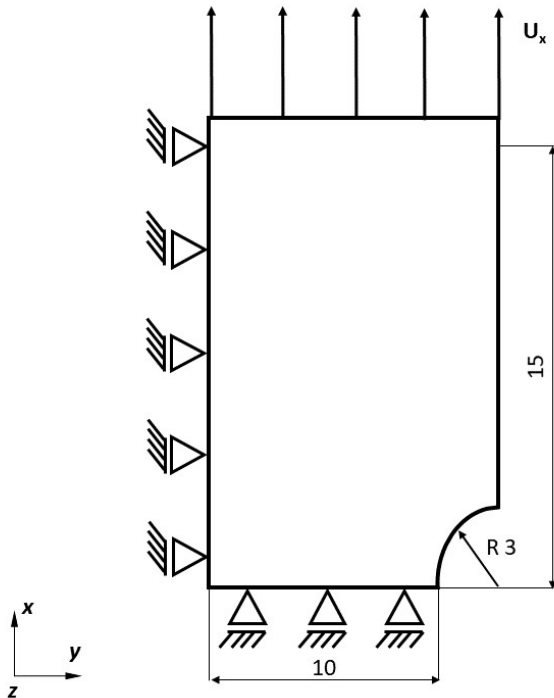


Figure 5.12: Specimen geometry and boundary conditions. Dimensions are given in mm. Displacement controlled loading  $U_x$  is applied.

The force-displacement response for the three different meshes with and without the regularization (Section(4.4)) schemes have been plotted in Figure (5.14a) and (5.14b) respectively. The global force-displacement response is characterized by a large linear regime followed by a gradual drop of the load (because of the softening) or a sudden drop in case of no regularization. From Figure (5.14), it is clearly evident that the model with regularization gives a more stable force-displacement response

compared to the model without regularization, where the maximum load capacity is very low, and the load drops significantly with the decrease in mesh size (i.e., increase in the number of elements). Even though the regularization scheme does not fully alleviate the mesh dependency, it improves the solution significantly compared to the material model without regularization.

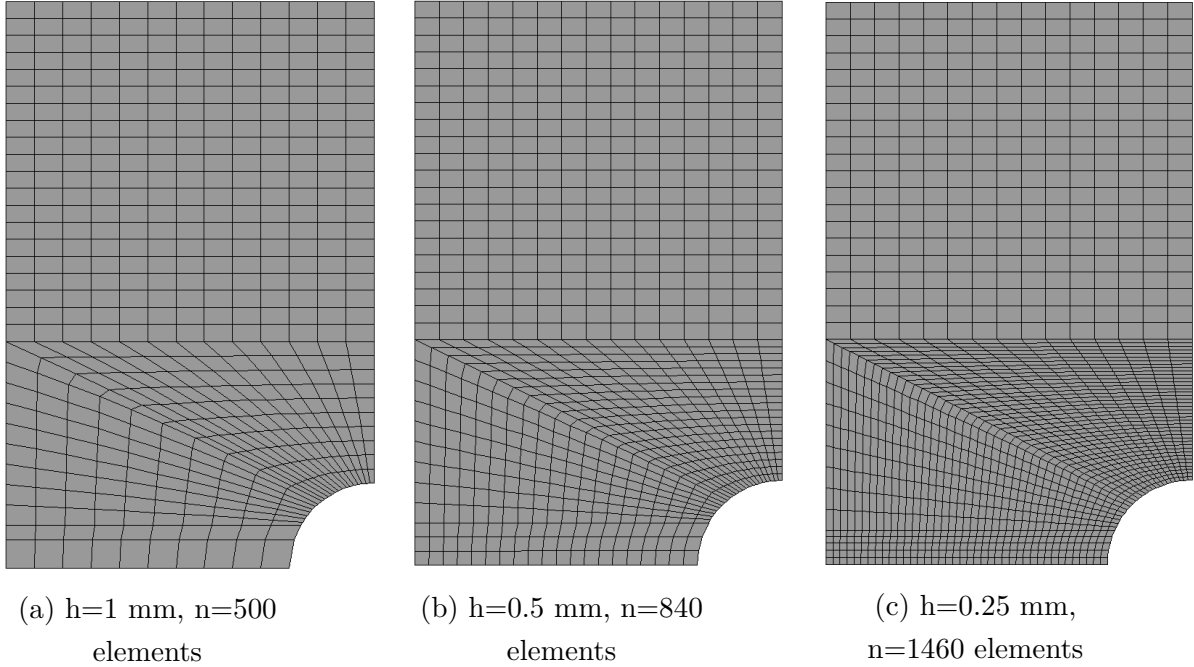


Figure 5.13: Considered meshes ( $h$  is the length of the element along fracture zone and  $n$  the total number of elements)

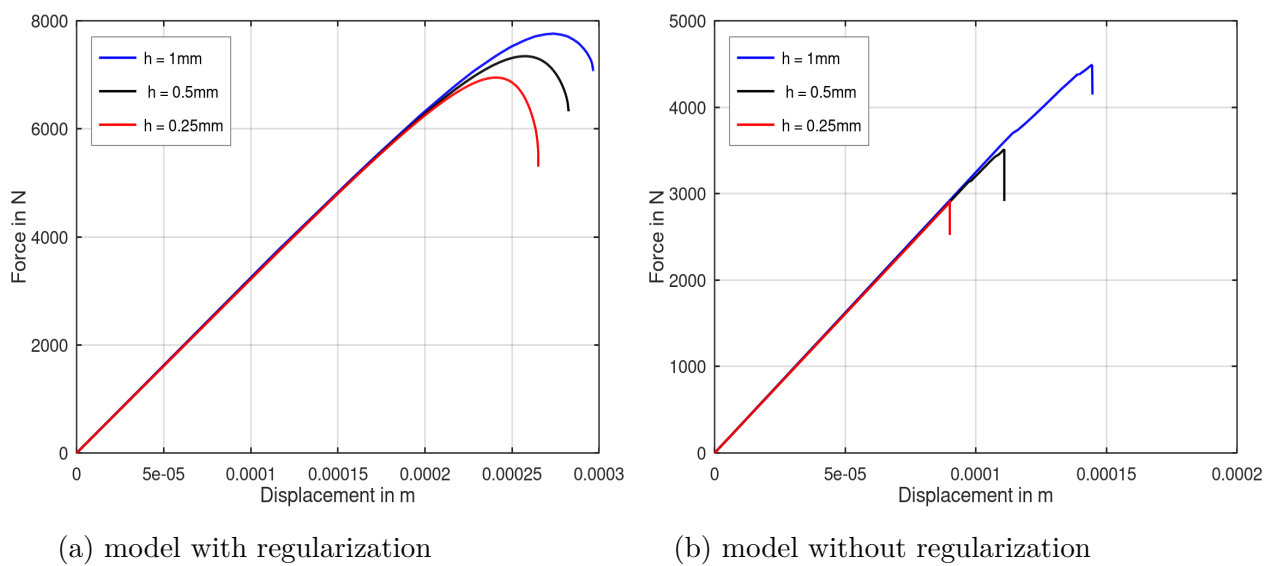
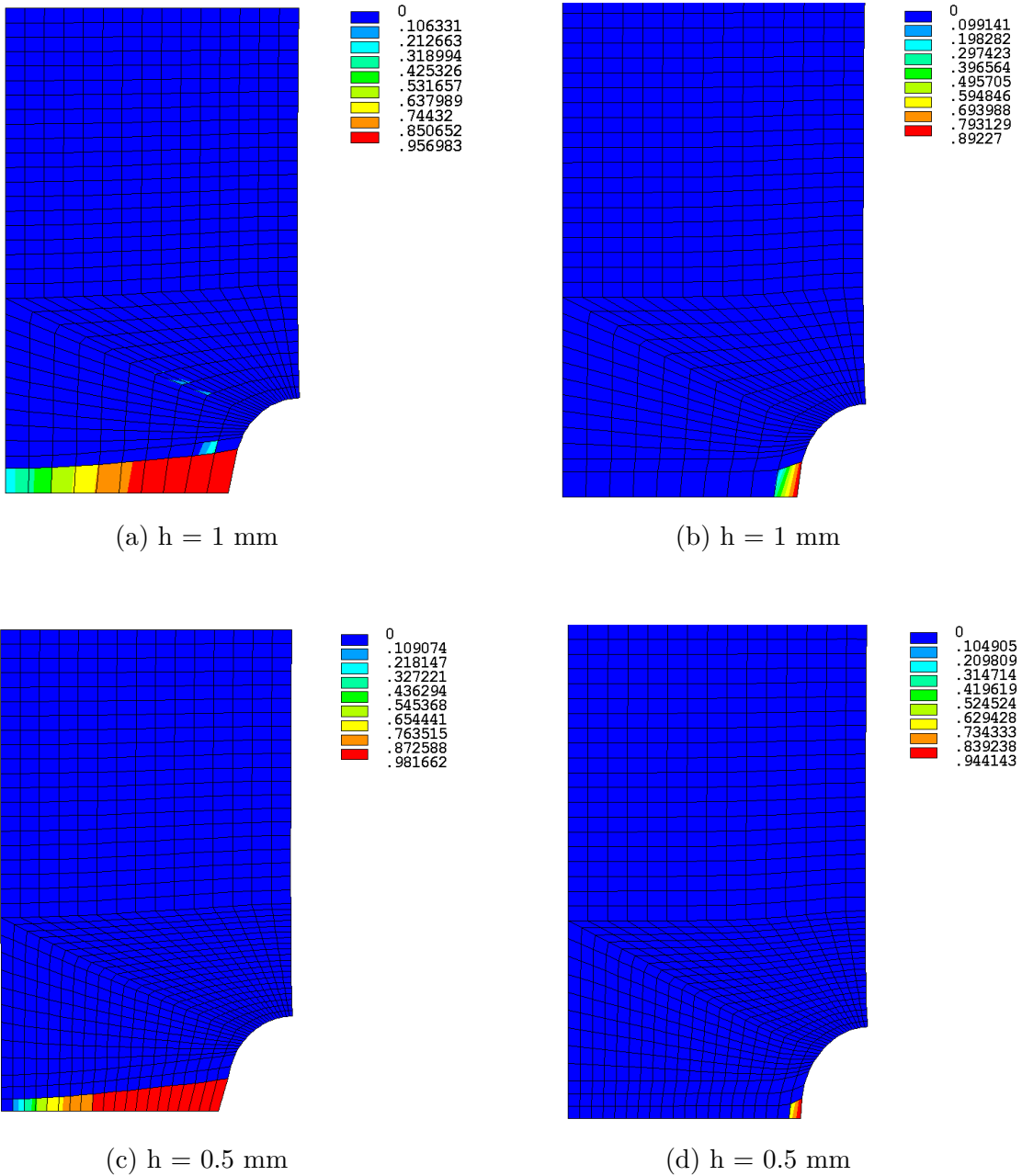
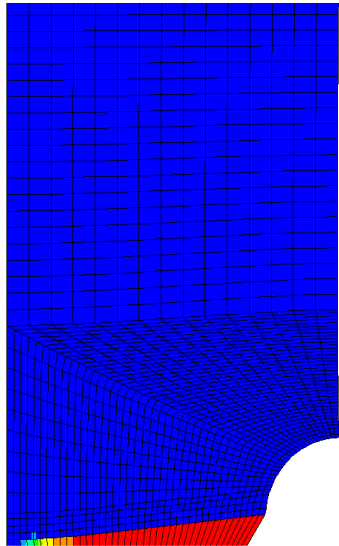


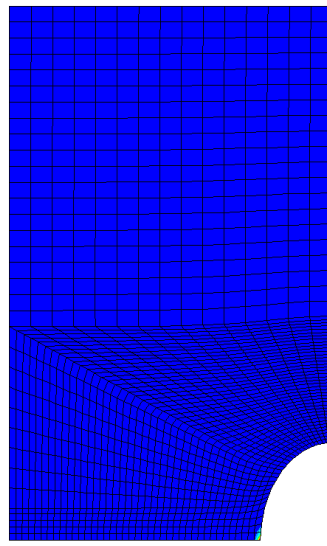
Figure 5.14: Convergence study: Global force-displacement response for model with regularization (Figure a on the left) and without regularization (Figure b the right)

The damage distributions at the end of the process have been plotted for the three different meshes in the Figure (5.15). For numerical reasons the maximum damage is limited to a threshold value of  $d_{max} = 0.999$ . The improvement in the global response by using regularization schemes has been illustrated by the damage distributions at the end of the loading process. A relatively large portion of the fracture zone takes part in the damage process instead of very few elements (one or two elements) in the case of no regularization. Damage initiates at the tip of the blunt notch and propagates perpendicular to the loading direction. The width of the damage zone is approximately the same in the three discretizations, but the number of elements that reach a critical damage value (red) increases with the increase in the number of elements along the fracture zone.





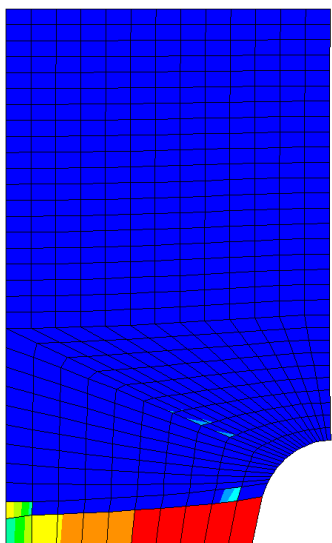
(e)  $h = 0.25 \text{ mm}$



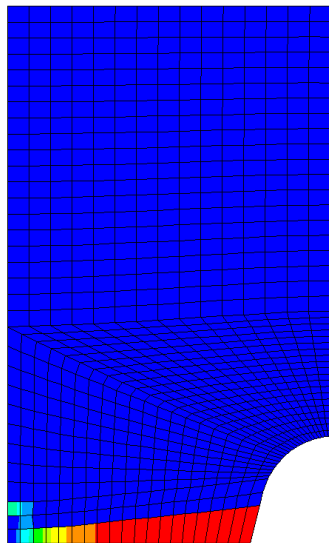
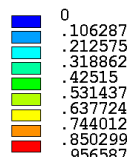
(f)  $h = 0.25 \text{ mm}$

Figure 5.15: Convergence study for model with(Figure a,c,e) and without(b,d,f) regularization: Damage contour plots  $d_1$  at the end of the loading

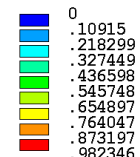
Now the transverse direction is kept parallel to the loading direction, and the behaviour of the damage model, i.e., initiation and propagation of damage  $d_2$ , is analysed by applying a tensile load in the transverse direction. The damage ( $d_2$ ) at the end of the loading process is shown in the Figure (5.16)

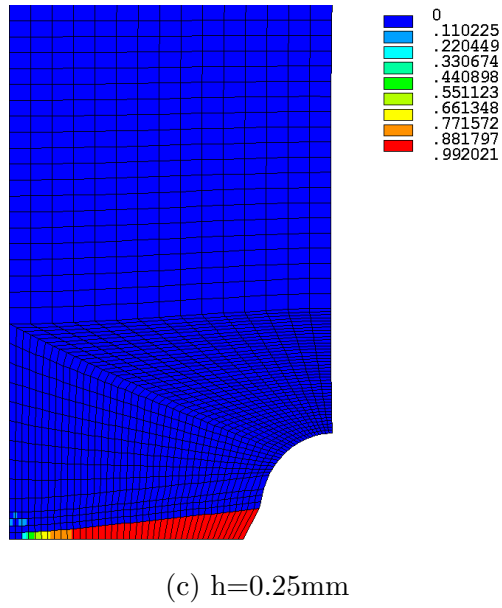


(a)  $h=1\text{mm}$



(b)  $h=0.5\text{mm}$





(c)  $h=0.25\text{mm}$

Figure 5.16: Damage contour plots  $d_2$  at the end of the loading (Loading in transverse direction)

The damage pattern looks similar to the distribution of damage ( $d_1$ ) when loaded in the longitudinal direction. The force-displacement response of both longitudinal and transverse loading for a single mesh type ( $h = 0.5\text{mm}$ ) is compared in the Figure (5.17). As expected, the maximum load capacity is high in the longitudinal direction compared to the transverse direction.

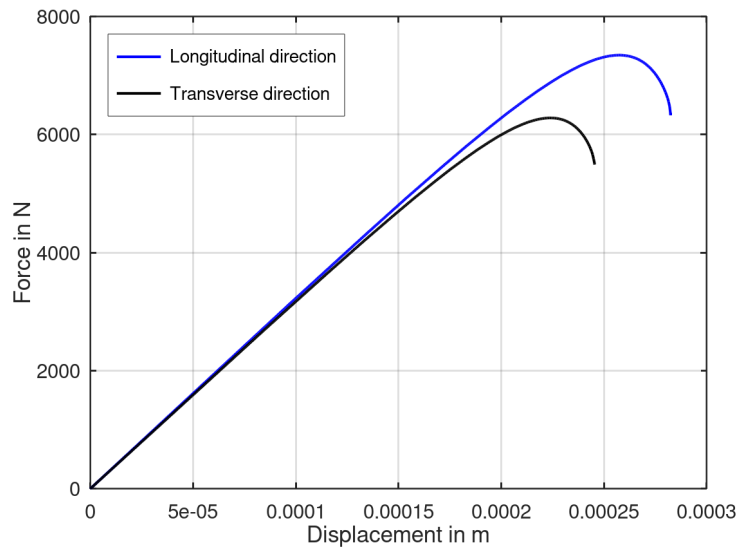


Figure 5.17: Comparison of force-displacement response in longitudinal and transverse direction for  $h=0.5\text{mm}$  discretization

### 5.3.2 Compact Tension (CT) Specimen

This second example demonstrates the model's ability to compute multiple damage variables simultaneously, i.e., show the anisotropic damage development when a load is applied. In the plane stress (2D) setting, two damage variables ( $d_1$  and  $d_2$ ), one in each principal direction, are employed to represent the anisotropic damage development. The Compact Tension test is a standard test for plane fracture of materials and the measurement of fatigue crack growths. Because of the symmetry, only one half of the specimen is modelled, and the geometry and appropriate boundary conditions (Peerlings, 1999) are given in Figure (5.18). The mesh consists of plane stress (PLANE 182) elements with bilinear interpolations for displacements, and  $2 \times 2$  Gauss integration has been utilized. Just like the notched tensile specimen, three different finite element meshes have been used in the fracture zone with the elements of size  $h = 1$  mm, 0.5 mm and 0.25 mm and a total of 509, 1409, 4811 elements, respectively for the convergence studies (Figure 5.19). A node is created at the centre of the pinhole, and the innermost nodes of the pinhole contour are connected to this node by rigid coupling option in ANSYS. A displacement controlled load ( $U_x$ ) is applied at the central node, and the global force-displacement response can be obtained from this central node. At first, the longitudinal direction is kept parallel to the loading direction, and the behaviour of the model is analyzed.

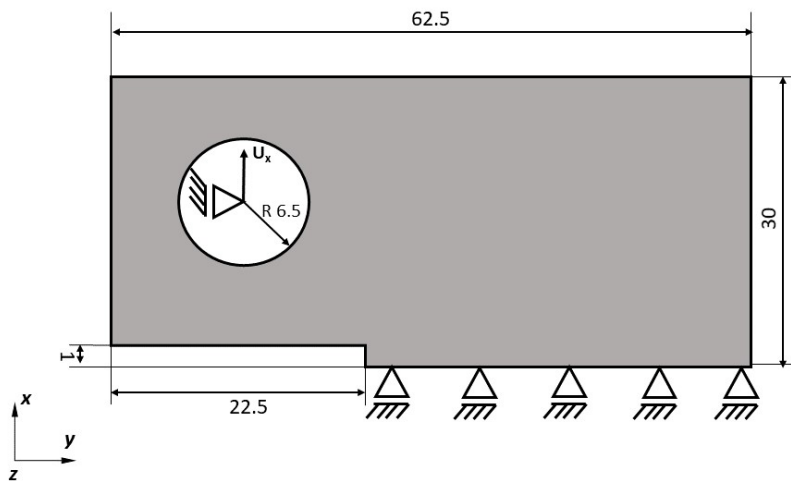
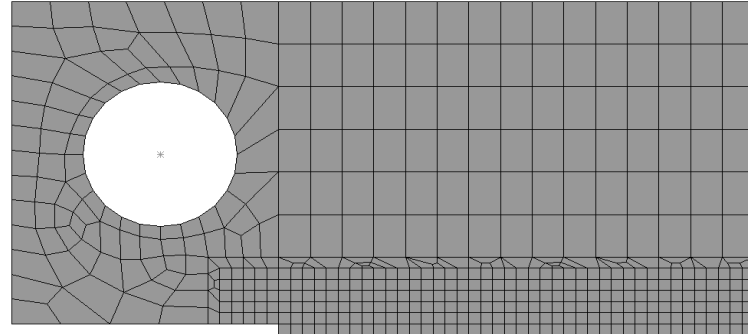


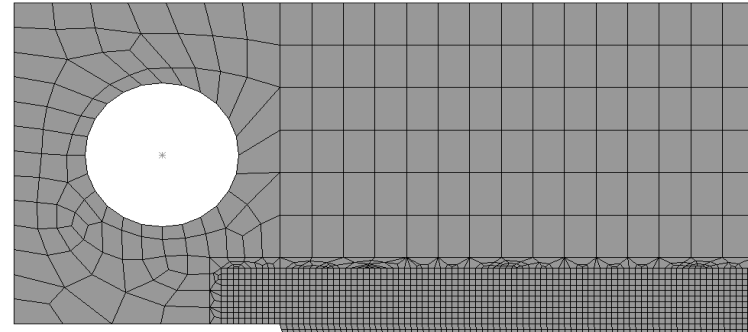
Figure 5.18: Specimen geometry and boundary conditions. Dimensions are given in mm. Displacement controlled loading  $U_x$  is applied

The global force-displacement response has been plotted for the three different meshes in Figure (5.20). As expected, the maximum load capacity decreases slightly with the decrease in mesh size (i.e., increase in the number of elements) because of the mesh sensitivity. The distributions of the damage variables  $d_1$  and  $d_2$  at the end of the loading process for the three different meshes have been plotted

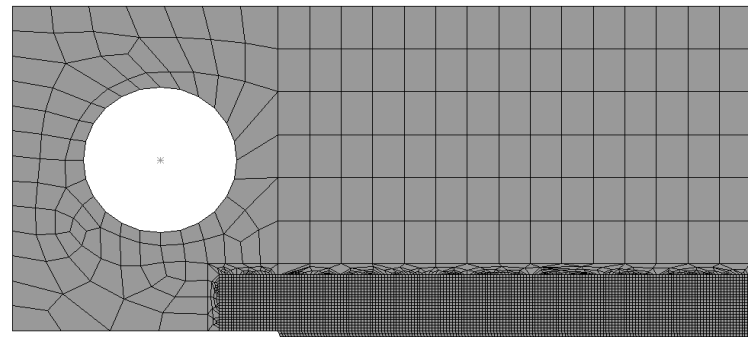
in Figure (5.21). The damage  $d_1$  is caused by tension in the longitudinal direction and  $d_2$  by tension in the transverse direction. The width of the damage zone for  $d_1$  is approximately the same in all three discretizations. When the damage  $d_1$  reaches the maximum threshold value in almost all the distorted elements, the simulations terminates; therefore, the maximum value and distribution of the damage variable  $d_2$  depends on the size of the elements. From Figures (5.21b), (5.21d) and (5.21f) it is clearly evident that the maximum value and the width of the damage zone for  $d_2$  increases with decrease in mesh size.



(a)  $h=1 \text{ mm}$



(b)  $h=0.5 \text{ mm}$



(c)  $h=0.25 \text{ mm}$

Figure 5.19: Considered meshes ( $h$  is the length of the element along fracture zone and  $n$  the total number of elements)

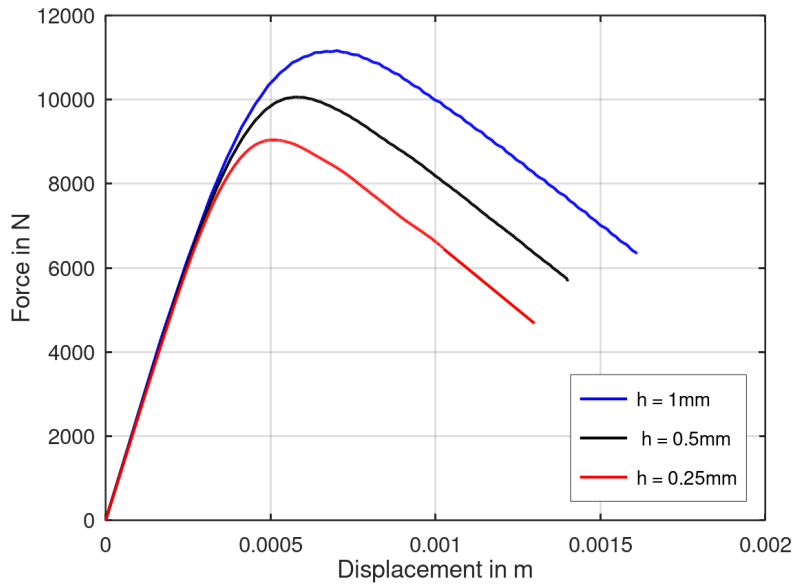
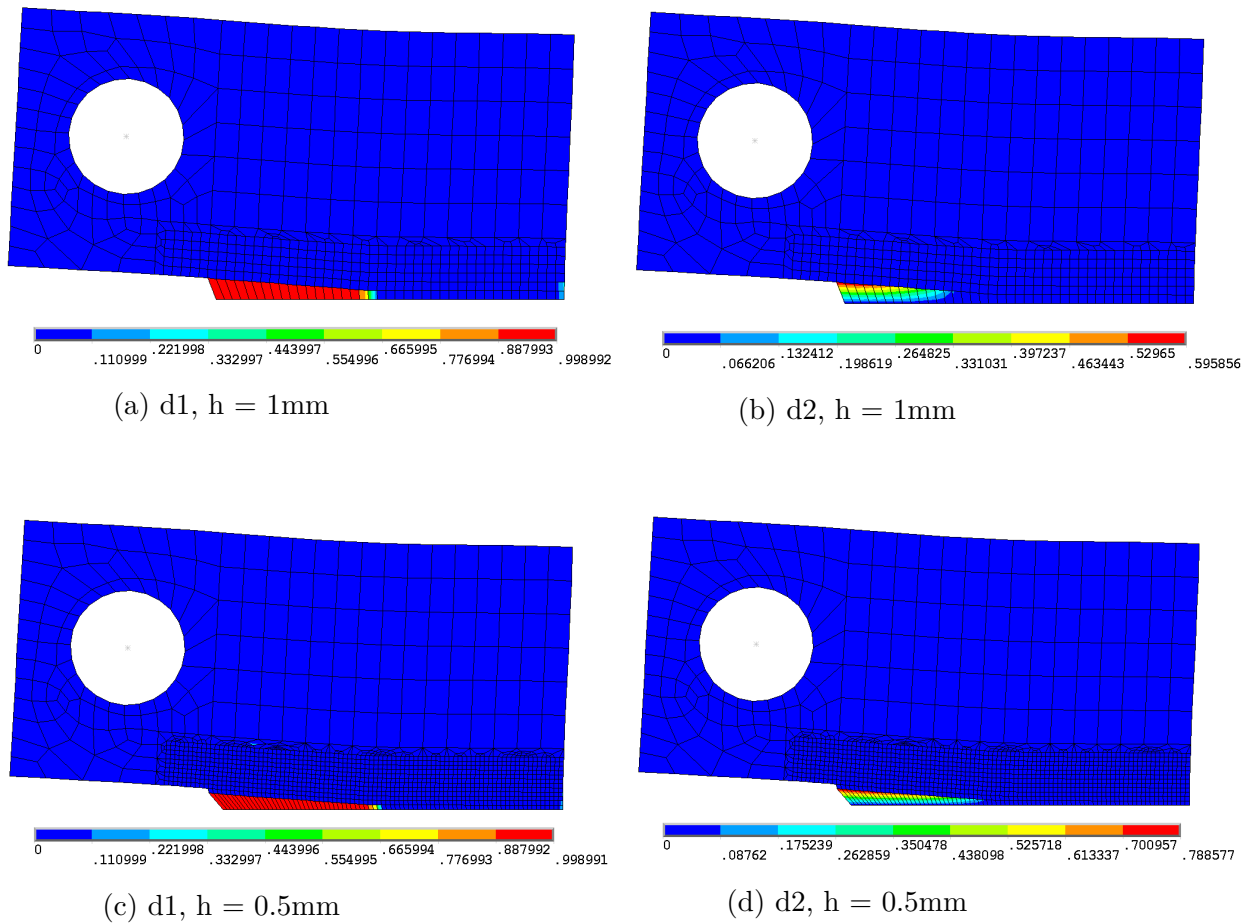
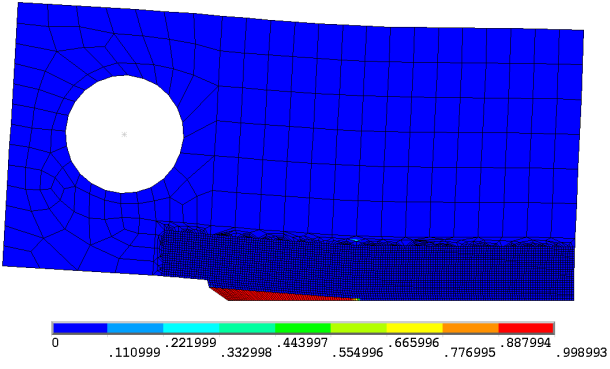
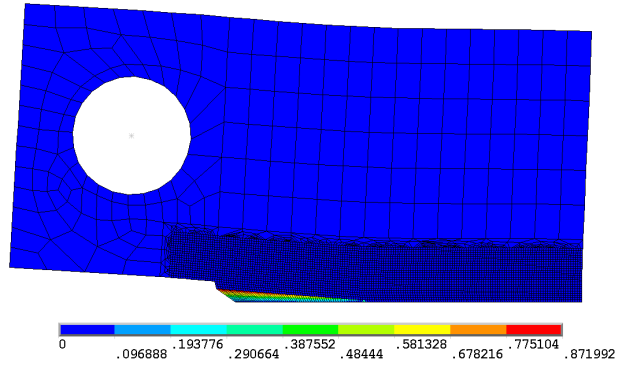


Figure 5.20: Convergence study: Global force-displacement response for three different meshes





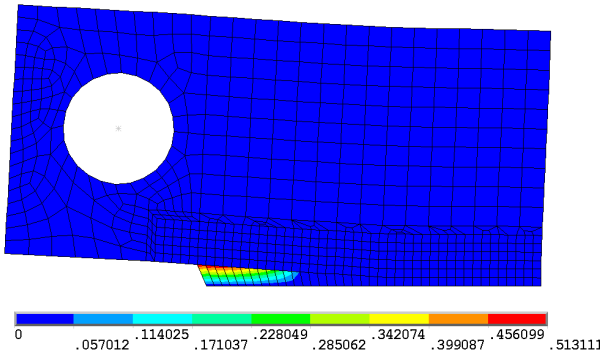
(e)  $d_1$ ,  $h = 0.25\text{mm}$



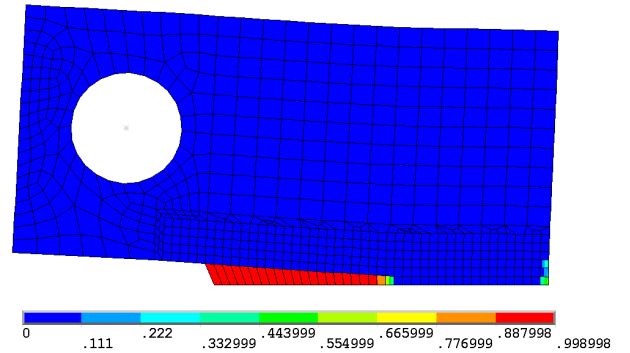
(f)  $d_2$ ,  $h = 0.25\text{mm}$

Figure 5.21: Damage distributions at the end of loading in longitudinal direction: Damage contour plots  $d_1$  and  $d_2$

Now the transverse direction is kept parallel to the loading direction, and the anisotropic development of damage  $d_1$  and  $d_2$  is analysed. In this case, damage  $d_2$  is the primary damage variable and damage  $d_1$  is dependent on the mesh size. The damage distributions ( $d_1$  and  $d_2$ ) for loading in transverse direction and force-displacement comparison of longitudinal and transverse loading for  $h=1\text{mm}$  discretization are shown in figure (5.22) and (5.23) respectively.



(a)  $d_1$



(b)  $d_2$

Figure 5.22: Damage distributions at the end of loading in transverse direction: Damage contour plots  $d_1$  and  $d_2$  ( $h = 1\text{mm}$  discretization)

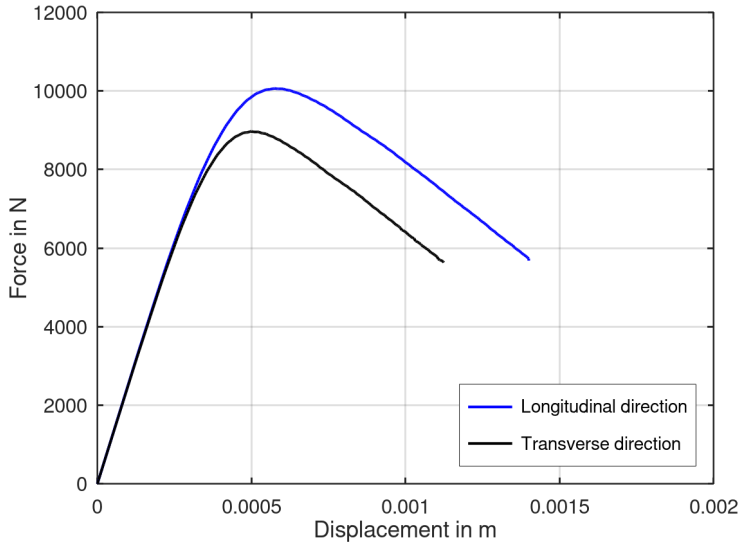


Figure 5.23: Comparison of force-displacement response in longitudinal and transverse direction for  $h = 1$  mm discretization

#### Effect of shear in damage development

To deeply understand the failure of composite materials, the effect of shear on damage initiation and propagation is studied. The effect of shear stress in each failure mechanism is introduced by the modified Hashin's failure criterion (Section (4.2.3)) where  $\alpha$  is the shear contribution factor which ranges from 0 to 1. The effect of shear can be studied by varying this shear contribution factor  $\alpha$ .

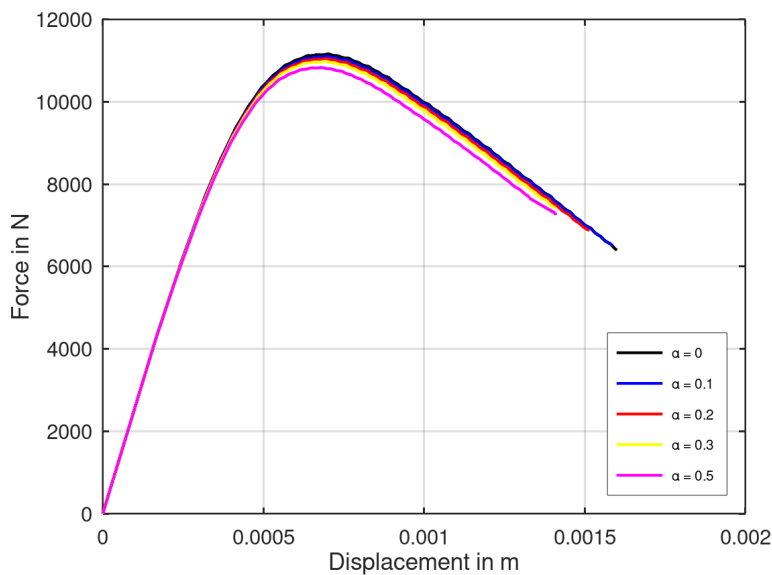


Figure 5.24: Comparison of force-displacement response for different shear coefficient ( $\alpha$ ) ( $h= 1$ mm discretization)

The maximum value of  $\alpha$  is chosen to be 0.5 to avoid the damage development only due to shear because the shear strength is low compared to other strengths. The global force-displacement response for different  $\alpha$  by loading the CT-Specimen in the longitudinal direction is shown in Figure (5.24). It is evident that by increasing  $\alpha$ , the failure index increases, which reduces the maximum load capacity of the CT specimen.

From Figure (5.25), it is clear that the increase in shear contribution has little to no effect in the initiation and distribution of the damage  $d_1$  because the shear stress component ( $\sigma_{12}$ ) is very low compared to the stress component ( $\sigma_{11}$ ) which is responsible for damage  $d_1$ . However, the shear stress ( $\sigma_{12}$ ) affects the damage  $d_2$  because its magnitude is significant compared to the stress component ( $\sigma_{22}$ ) which is the only component responsible for damage  $d_2$  in the case of the maximum stress criterion previously employed.

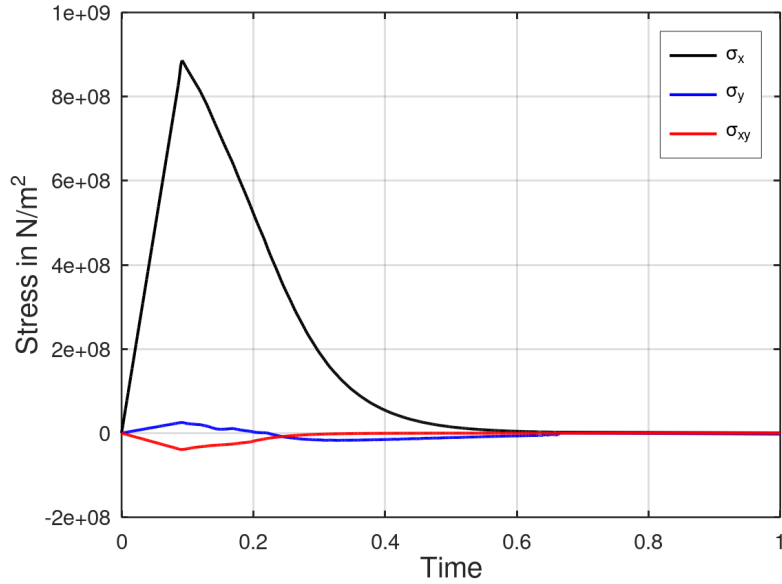


Figure 5.25: Evolution of stress components during longitudinal tensile loading ( $h=1\text{mm}$  discretization)

The contour plots of damage  $d_2$  for increasing shear contribution are plotted in Figure (5.26). Compared to no shear effect ( $\alpha = 0$ ), the model with the presence of shear effect has more realistic damage propagation of ( $d_2$ ), and the width of the damage zone is significantly larger. For the model with shear effect, the width of the damage zone is almost similar in all the cases, but the maximum damage value and the number of elements reaching critical damage value increase with the increase in  $\alpha$ .

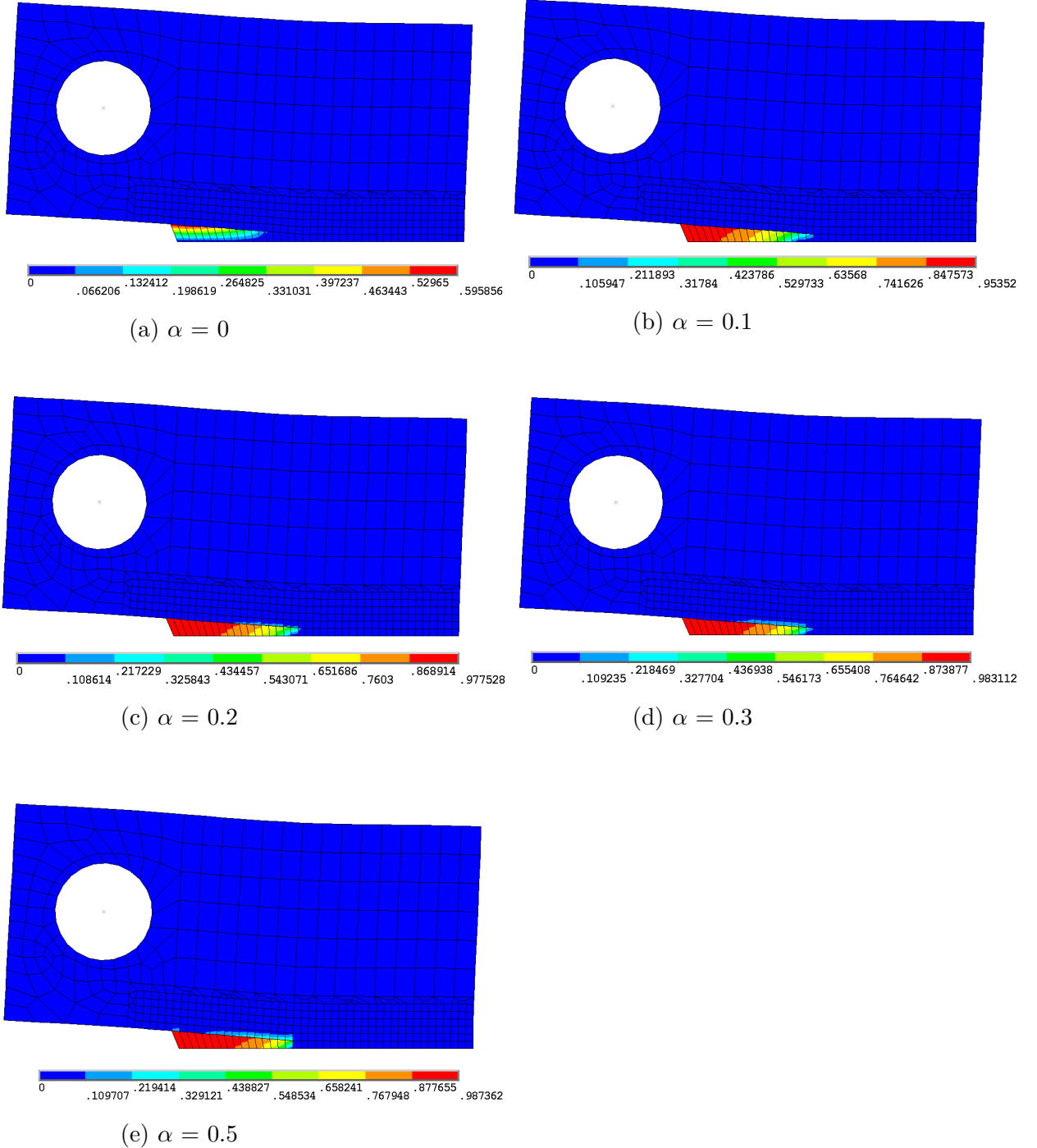


Figure 5.26: Damage distributions at the end of longitudinal loading: Damage contour plots  $d_2$  for different shear co-efficients ( $\alpha$ )

In the case of transverse loading, the damage  $d_2$  is unaffected because the magnitude of the shear stress ( $\sigma_{12}$ ) is very low compared to the stress ( $\sigma_{22}$ ). However, the damage  $d_1$  is affected because the magnitude of the shear stress component ( $\sigma_{12}$ ) is similar compared to ( $\sigma_{11}$ ).

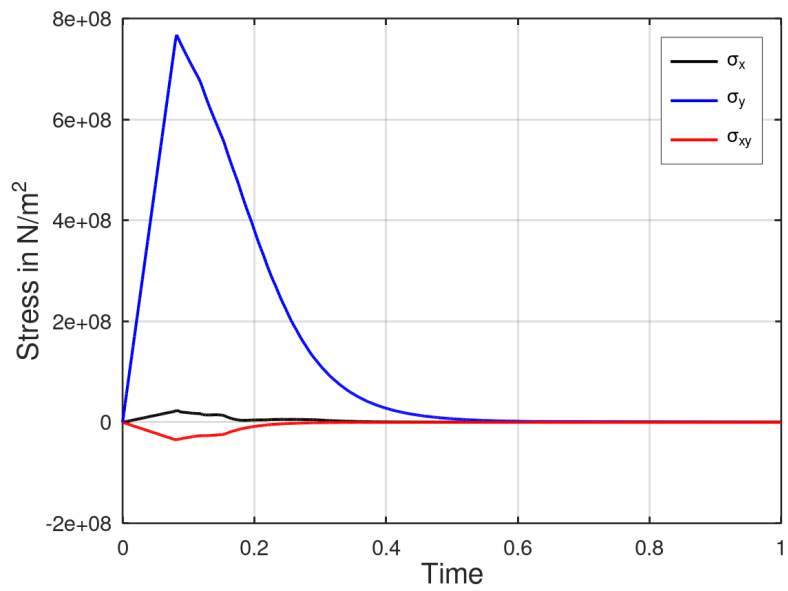


Figure 5.27: Evolution of stress components during transverse tensile loading ( $h=1\text{mm}$  discretization)

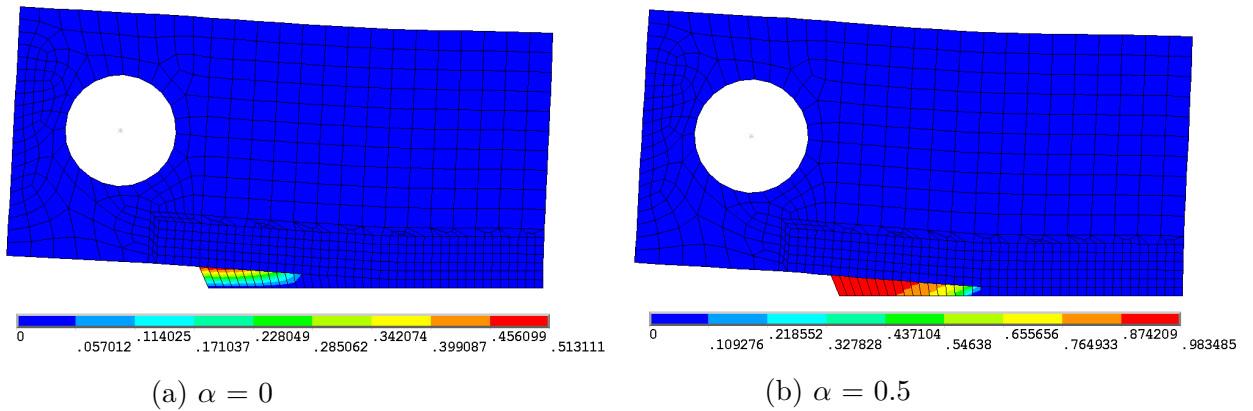


Figure 5.28: Damage distributions at the end of transverse loading: Damage contour plots  $d_1$  for different shear co-efficient ( $\alpha$ )

### 5.3.3 Plate with hole (3D)

This third example demonstrates the model's ability to show the anisotropic damage development for three dimensional (3D) problems. In 3D, three damage variables ( $d_1$ ,  $d_2$  and  $d_3$ ) are employed to represent the anisotropic damage development, i.e., one damage variable for each principal material direction. Because of symmetry, only one-eighth of the specimen has been modelled. The geometry and the appropriate boundary conditions are given in Figure (5.29). Eight node solid elements (SOLID 185) with trilinear interpolations of the displacements and full integration has been used to perform the FE modelling. The thickness was divided into four elements, and a fine mesh has been used in the region closer to the fracture zone shown in the Figure (5.30).

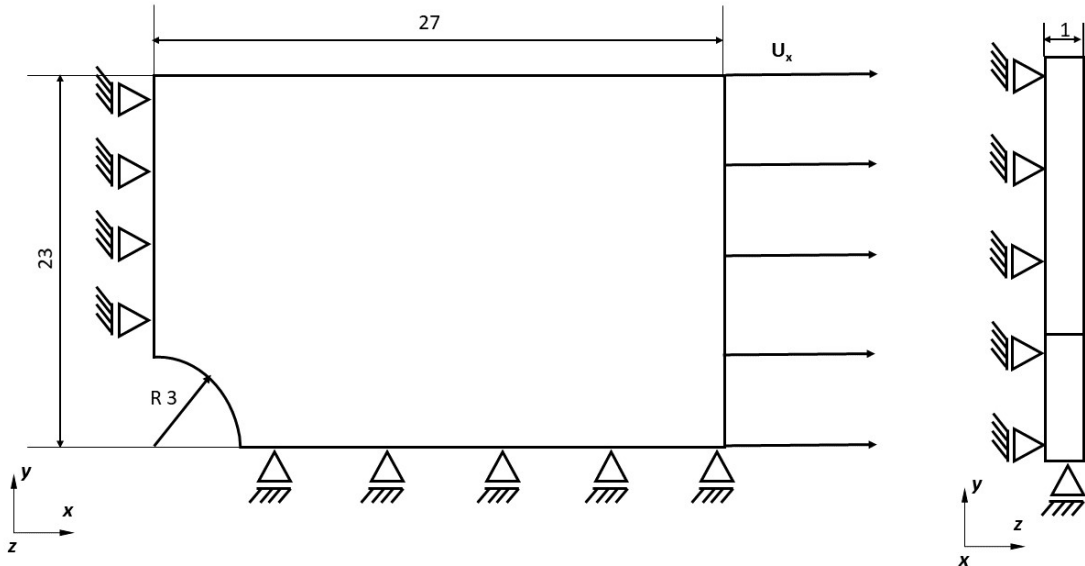


Figure 5.29: Specimen geometry and boundary conditions. Dimensions are given in mm. Displacement controlled loading  $U_x$  is applied

The longitudinal direction is kept parallel to the loading direction, and the behaviour of the model is analysed by applying displacement controlled load ( $U_x$ ) in the longitudinal direction (X-direction). The strength in transverse directions (2 and 3) are large enough for the damage variables  $d_2$  and  $d_3$  not to initiate when a longitudinal tensile load is applied. So to demonstrate the model's capability to show anisotropic damage development the transverse strength has been reduced (For both tension and compression). The material properties considered for 3D damage model () are given in the Table. (5.3). The maximum stress criterion (See Section(4.2.2)) has been used to predict the damage initiation in the three principal material directions.

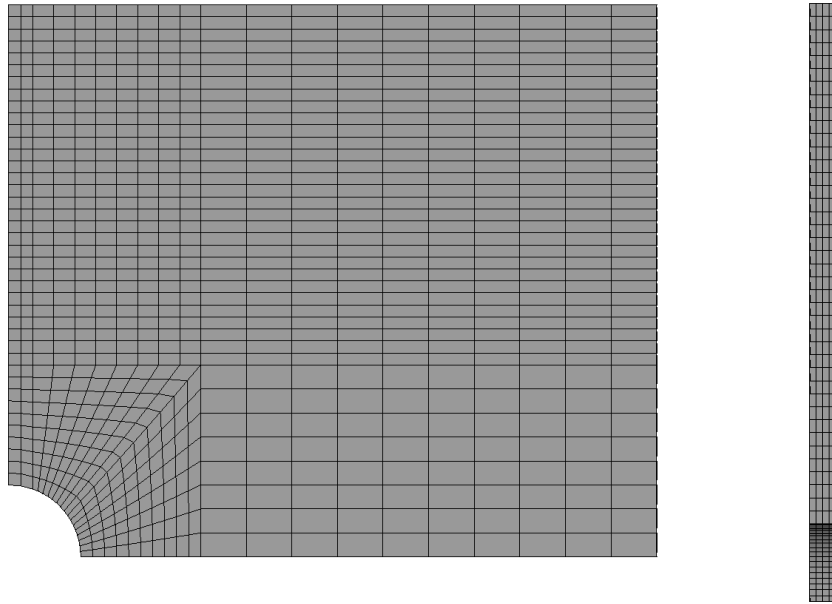


Figure 5.30: Finite element discretization used for 3D damage study

Symbol	Material Parameter	Value
$E_{11}$	Modulus in longitudinal (1) direction	55.8 GPa
$E_{22} = E_{33}$	Modulus in transverse (2 and 3) directions	54.9 GPa
$\nu_{12} = \nu_{13}$	Poisson's ratio	0.043
$G_{12} = G_{23} = G_{13}$	Shear modulus	4.2 GPa
$X_t$	Tensile strength in longitudinal (1) direction	910.1 MPa
$X_c$	Compressive strength in longitudinal (1) direction	-710.2 MPa
$Y_t$	Tensile strength in (2 and 3) directions	300 MPa
$Y_c$	Compressive strength in (2 and 3) directions	-300 MPa
$S_{12}$	In-plane strength	131 MPa
$G_f^{lt}$	Tensile fracture energy along longitudinal (1) direction	125 KJ/m <sup>2</sup>
$G_f^{lc}$	Compressive fracture energy along longitudinal (1) direction	250 KJ/m <sup>2</sup>
$G_f^{tt}$	Tensile fracture energy along (2 and 3) directions	95 KJ/m <sup>2</sup>
$G_f^{tc}$	Compressive fracture energy along (2 and 3) directions	254 KJ/m <sup>2</sup>

Table 5.3: Material parameters (3D Damage model)

The global force-displacement response has been plotted for this longitudinal tensile loading in Figure (5.31). The response is similar to the longitudinal loading in the notched tensile specimen, being characterized by a linear regime followed by a gradual drop of the load because of the softening. The softening is observed to initiate when the damage happens in critical number of elements in the fracture zone.

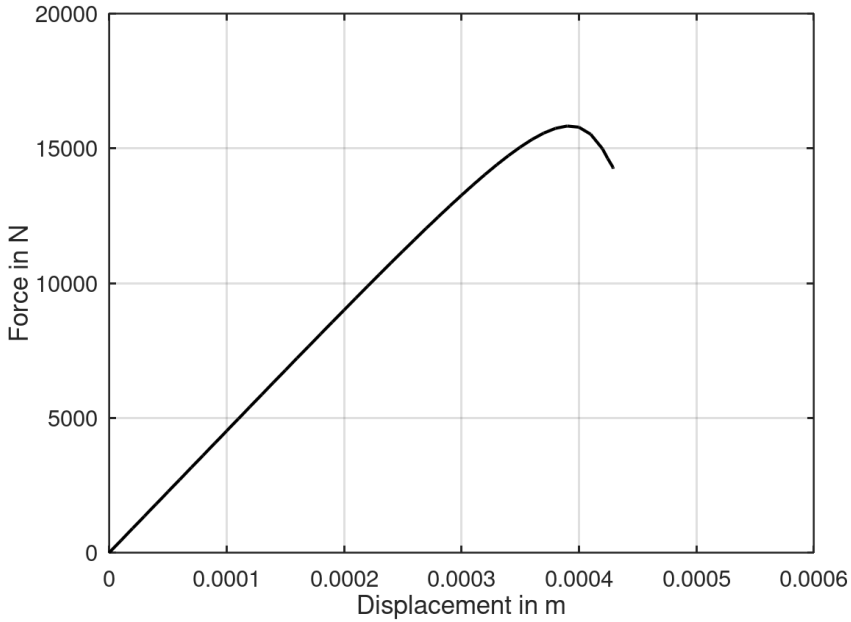
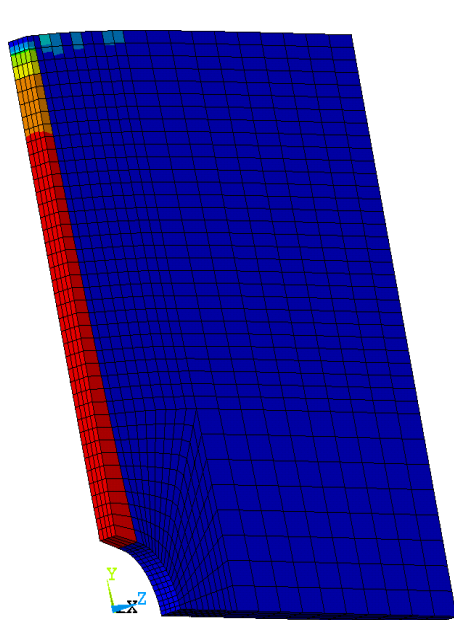


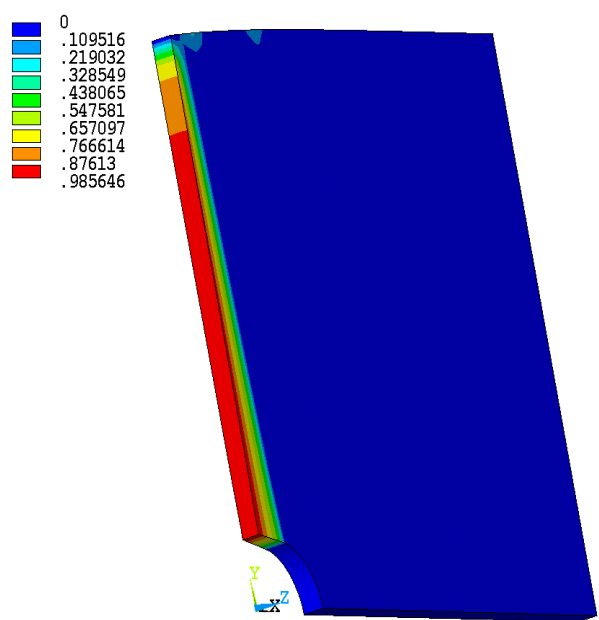
Figure 5.31: Global force-displacement response for the longitudinal tensile loading

The damage distribution ( $d_1$ ,  $d_2$  and  $d_3$ ) at the end of the tensile loading is shown in the Figure (5.32). In order to get a good visualization and understanding both element and nodal solution values of the damage are plotted. The initiation and evolution of damage  $d_1$  is caused by the normal stress component  $\sigma_{11}$  in the longitudinal direction. The damage  $d_1$  initiates at the tip of the blunt notch and then propagates perpendicular to the loading direction.

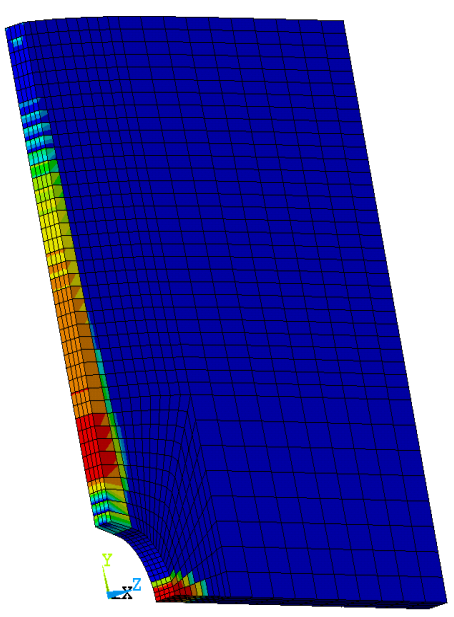
From Figures (5.32c) and (5.32d) it is evident that the damage happens at two separate regions, i) perpendicular to the loading direction where damage  $d_1$  already propagated ii) right at the blunt notch at the bottom edge of the plate. It has been observed that the damage  $d_2$  in the region (i) happens because of tension in the transverse direction, and in the region (ii) the damage is caused by the compression in the transverse direction. The propagation of damage  $d_3$  is caused by the normal stress component  $\sigma_{33}$  in the thickness direction. The damage  $d_2$  and  $d_3$  has much lesser influence on the strength of the specimen compared to the damage  $d_1$  during longitudinal tensile loading.



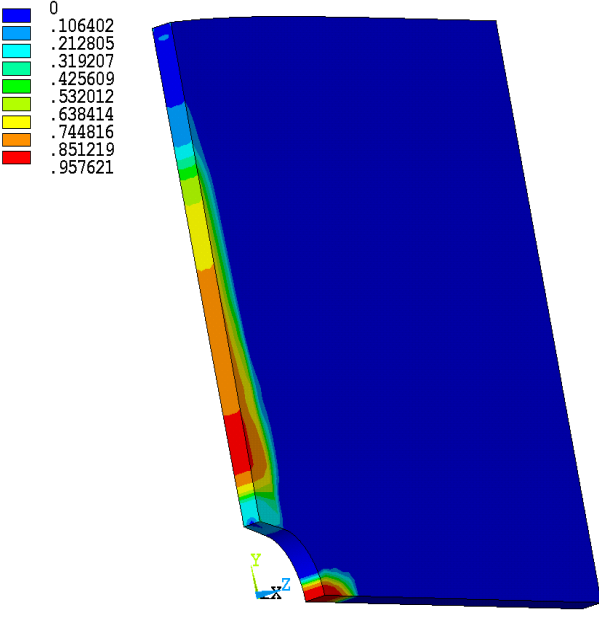
(a) Damage  $d_1$  - Element solution



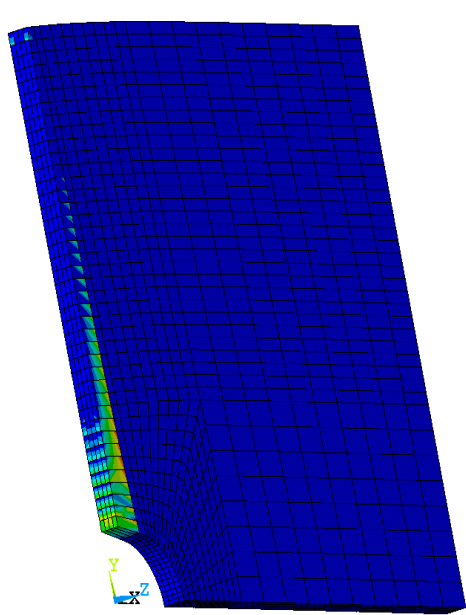
(b) Damage  $d_1$  - Nodal solution



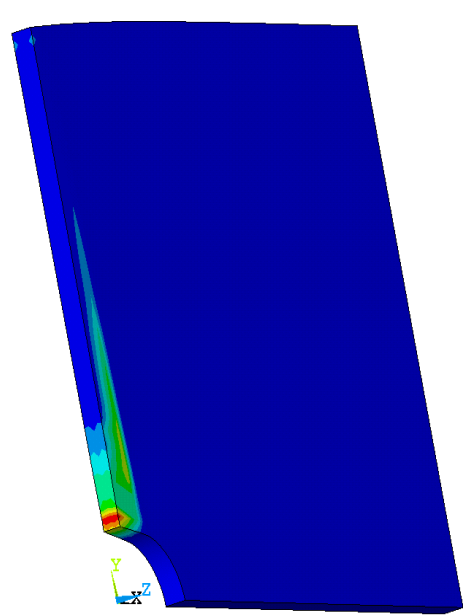
(c) Damage  $d_2$  - Element solution



(d) Damage  $d_2$  - Nodal solution



(e) Damage  $d_3$  - Element solution



(f) Damage  $d_3$  - Nodal solution

Figure 5.32: Contour plots of the damage distribution  $d_1$ ,  $d_2$  and  $d_3$  at the end of longitudinal tensile loading

These damage contour plots clearly indicate that the developed 3D model has the ability to show not only the damage development in three principal material directions but also both tension and compression damage happening simultaneously in a specimen when a load is applied.

# Chapter 6

## Summary and Conclusion

The main objective of this work is to develop progressive damage models which can clearly describe the damage mechanism in orthotropic composite materials when subject to various loading conditions. The models are developed using the framework of continuum damage mechanics (CDM). A second-order orthotropic damage tensor is employed to show the anisotropic damage development. A key issue in damage modelling is the convergence issue that arise due to the mesh dependant behaviour of the strain-softening models. To reduce the mesh sensitivity, fracture energy regularization technique has been employed which ensures the objectivity of the model by adjusting dissipated energy to each finite element. At first the damage models (both 2D/Plane-stress and 3D cases) are implemented in octave and tested using constitutive driver routines for simple loading cases to verify the numerical implementation, and to understand the behaviour of the material at integration point level i.e., damage-evolution and strain-softening. During the integration point studies it has been observed that the failure criteria which uses strain to predict the damage initiation causes convergence issues when damage evolves without the presence of stress in the given material direction i.e., when transverse strength is very low and an uniaxial tension is applied in longitudinal direction. So the damage models implemented as user-defined material routines (USERMAT) in ANSYS employs stress-based damage initiation criteria

The user-defined material routines (USERMAT) are tested using a finite element of unit length in ANSYS in order to compare against the results from octave implementation. Once verified, representative structural examples (both 2D and 3D) are used to test the damage models in ANSYS to see how they predict the initiation and evolution of damage under various circumstances. Finite elements of varying sizes are used in the area prone to damage to analyse the mesh sensitivity of the damage models. It has been observed that the employed regularization scheme significantly improves the global response but it does not fully alleviate the mesh dependency problems which arise due to strain-softening. Therefore a drop in max-

imum load capacity i.e., reduction in energy dissipation, is observed in the global force-displacement response when the mesh is refined. Different failure criteria has been employed to see how the damage initiation and failure indices affect the model. It has been observed that the inclusion of shear effect naturally reduces the maximum load capacity because of the increase in failure index for the same load. In some cases the shear effect improves the damage propagation and distribution when the magnitude of shear stress is significant compared to the normal stresses in the given material direction. Finally the implemented damage models employing exponential damage evolution laws have the ability to represent the anisotropic damage development with the help of a second-order damage tensor and the strain-softening which results due to the stiffness degradation in both 2D and 3D cases. This work provides a better understanding of the numerical implementation of the anisotropic damage models which can predict the damage behaviour of complex composite materials.

The following changes and developments can be made in future to make this anisotropic damage model an excellent tool to analyze the complex damage phenomena in composite-materials used in real-life applications

- By incorporating complex failure criteria like Linde's failure criteria, Hashins quadratic failure criteria (Jiang et al., 2018) etc., the damage initiation and propagation can be predicted more accurately because of the inclusion of shear effects and quadratic terms.
- From section (5.3.2) (CT-Specimen) it is evident that when most of the distorted elements reaches a critical value the simulation terminates. This has been the case in most of the work done before. But in very few works (Jiang et al., 2018), (Sokolinsky et al., 2011) an option called element deletion (Available in the FEM software Abaqus) is employed to delete a particular failed element when the damage reaches a critical threshold value. This option can be included in the future to avoid the premature termination of analysis and the whole crack propagation in the case of CT specimen can be simulated.
- Non-local gradient-enhanced damage formulations can be incorporated into the anisotropic damage models to eliminate the mesh dependency problems encountered in this work. These non-local models uses weighted volume averages of the state variables to create spatial interactions which induces smoothing effect on the deformation and damage. Gradient enhanced formulations uses higher-order deformation gradients of internal variables to create spatial discretization thereby eliminating the mesh dependency. Some of the works based on non-local damage models are (Peerlings, 1999), (Fassin et al., 2019), (Geers, 1998), (Seupel et al., 2018)

# Bibliography

B.Kiefer. Constitutive driver routines. Driver routines provided during the plasticity course (CMS) for testing the implemented material models. [coded by: B. Kiefer 15 Nov 2011, analytical solution added: S. Prueger 10 Dec 2018].

Brainkart. Uni, Bi and Triaxial tension. [https://www.brainkart.com/article/Triaxial-Stress,-Biaxial-Stress,-and-Uniaxial-Stress\\_5991/#:~:text=A%20two%2Ddimensional%20state%20of,called%20a%20uniaxial%20stress%20state](https://www.brainkart.com/article/Triaxial-Stress,-Biaxial-Stress,-and-Uniaxial-Stress_5991/#:~:text=A%20two%2Ddimensional%20state%20of,called%20a%20uniaxial%20stress%20state). [Online; accessed 20-August-2021].

Miguel Cervera and Michele Chiumenti. Smeared crack approach: back to the original track. *International journal for numerical and analytical methods in geomechanics*, 30(12):1173–1199, 2006.

JP Cordebois and F Sidoroff. Damage induced elastic anisotropy. In *Mechanical Behavior of Anisotropic Solids/Comportment Méchanique des Solides Anisotropes*, pages 761–774. Springer, 1982.

efunda. Elastic stiffness matrix of an orthotropic material . [https://www.efunda.com/formulae/solid\\_mechanics/mat\\_mechanics/hooke\\_orthotropic.cfm](https://www.efunda.com/formulae/solid_mechanics/mat_mechanics/hooke_orthotropic.cfm). [Online; accessed 5-June-2021].

Alaa El-Din A El-Sisi, Hesham M El-Emam, Hani A Salim, and Hossam El-Din M Sallam. Efficient 3d modeling of damage in composite materials. *Journal of Composite Materials*, 49(7):817–828, 2015.

BG Falzon and Paola Apruzzese. Numerical analysis of intralaminar failure mechanisms in composite structures. part i: Fe implementation. *Composite Structures*, 93(2):1039–1046, 2011.

Marek Fassin, Robert Eggersmann, Stephan Wulffinghoff, and Stefanie Reese. Gradient-extended anisotropic brittle damage modeling using a second order damage tensor-theory, implementation and numerical examples. *International Journal of Solids and Structures*, 167:93–126, 2019.

Marc Georges Denis Geers. Experimental analysis and computational modelling of damage and fracture. 1998.

Zvi Hashin. Analysis of composite materials—a survey. 1983.

Rodney Hill. Elastic properties of reinforced solids: some theoretical principles. *Journal of the Mechanics and Physics of Solids*, 11(5):357–372, 1963.

Hongyong Jiang, Yiru Ren, Zhihui Liu, Songjun Zhang, and Xiaoqing Wang. Evaluations of failure initiation criteria for predicting damages of composite structures under crushing loading. *Journal of Reinforced Plastics and Composites*, 37(21):1279–1303, 2018.

Lasar Kachanov. *Introduction to continuum damage mechanics*, volume 10. Springer Science & Business Media, 1986.

Ireneusz Lapczyk and Juan A Hurtado. Progressive damage modeling in fiber-reinforced materials. *Composites Part A: Applied Science and Manufacturing*, 38(11):2333–2341, 2007.

J Lemaitre and Jean-Louis Chaboche. Aspect phénoménologique de la rupture par endommagement. *J Méc Appl*, 2(3), 1978.

Jean Lemaitre. *A course on damage mechanics*. Springer Science & Business Media, 2012.

BM Lempriere. Poisson's ratio in orthotropic materials. *Aiaa Journal*, 6(11):2226–2227, 1968.

G Lin. Ansys user material subroutine usermat. *ANSYS, Canonsburg, PA*, 1999.

P Maimí, Pedro Ponces Camanho, JA Mayugo, and CG Dávila. A continuum damage model for composite laminates: Part i—constitutive model. *Mechanics of materials*, 39(10):897–908, 2007.

Sumio Murakami. *Continuum damage mechanics: a continuum mechanics approach to the analysis of damage and fracture*, volume 185. Springer Science & Business Media, 2012.

Ronnie Henricus Johannes Peerlings. Enhanced damage modelling for fracture and fatigue. 1999.

P.Nikethan. Composite materials in a Boeing 787 'Dreamliner'. <https://www.slideshare.net/nagababutallam/composite-materials-in-aerospace-industry>, 2016. [Online; accessed 5-August-2021].

Muhammad Masood Rafi, Ali Nadjai, and Faris Ali. Analytical modeling of concrete beams reinforced with carbon frp bars. *Journal of Composite Materials*, 41(22):2675–2690, 2007.

Andreas Seupel, Geralf Hütter, and Meinhard Kuna. An efficient fe-implementation of implicit gradient-enhanced damage models to simulate ductile failure. *Engineering Fracture Mechanics*, 199:41–60, 2018.

David W Sleight. *Progressive failure analysis methodology for laminated composite structures*. Citeseer, 1999.

Vladimir S Sokolinsky, Kyle C Indermuehle, and Juan A Hurtado. Numerical simulation of the crushing process of a corrugated composite plate. *Composites Part A: Applied Science and Manufacturing*, 42(9):1119–1126, 2011.

TWI. Composite materials. <https://www.twi-global.com/technical-knowledge/faqs/what-is-a-composite-material#:~:text=A%20composite%20material%20is%20a,also%20improve%20strength%20and%20stiffness.>, 2016. [Online; accessed 15-July-2021].

Yuequan Wang, Mingbo Tong, and Shuhua Zhu. Three dimensional continuum damage mechanics model of progressive failure analysis in fibre-reinforced composite laminates. In *50th AIAA/ASME/ASCE/AHS/ASC Structures, Structural Dynamics, and Materials Conference 17th AIAA/ASME/AHS Adaptive Structures Conference 11th AIAA No*, page 2629, 2009.

Wikipedia. Fibre-reinforced composite. [https://en.wikipedia.org/wiki/Fiber-reinforced\\_composite](https://en.wikipedia.org/wiki/Fiber-reinforced_composite). [Online; accessed 10-June-2021].



# Appendix

## A.1 Elastic stiffness matrix of the damaged material

### A.1.1 Plane stress (2D)

The elastic stiffness matrix of the damage material for transversely isotropic material has the form

$$\mathbb{C}(D) = \frac{1}{D} \begin{bmatrix} C_{11}(1-d_1) & C_{12}(1-d_1)(1-d_2) & 0 \\ C_{21}(1-d_2)(1-d_1) & C_{22}(1-d_2) & 0 \\ 0 & 0 & D(1-d_3)G_{12} \end{bmatrix}$$

where  $D = 1 - (1-d_1)(1-d_2)\nu_{12}\nu_{21}$  and  $d_3 = 1 - (1-d_1)(1-d_2)$

### A.1.2 3D

The elastic stiffness matrix of the damage material for orthotropic material has the form

$$\mathbb{C}(D) = \begin{bmatrix} C_{11}^d & C_{12}^d & C_{13}^d & 0 & 0 & 0 \\ C_{21}^d & C_{22}^d & C_{23}^d & 0 & 0 & 0 \\ C_{31}^d & C_{32}^d & C_{33}^d & 0 & 0 & 0 \\ 0 & 0 & 0 & C_{44}^d & 0 & 0 \\ 0 & 0 & 0 & 0 & C_{55}^d & 0 \\ 0 & 0 & 0 & 0 & 0 & C_{66}^d \end{bmatrix}$$

where  $C_{ij}^d = (1 - d_i)(1 - d_j)$ ,  $i, j = 1, 2, 3$

$$C_{44}^d = (1 - d_1)(1 - d_2),$$

$$C_{55}^d = (1 - d_1)(1 - d_3),$$

$$C_{66}^d = (1 - d_2)(1 - d_3)$$

```

1
2  subroutine usermat(
3      & matId, elemId, kDomIntPt, kLayer, kSectPt,
4      & ldstep, isubst, keycut,
5      & nDirect, nShear, ncomp, nStatev, nProp,
6      & Time, dTime, Temp, dTemp,
7      & stress, ustatev, dsdePl, sedEl, sedPl, epseq,
8      & Strain, dStrain, epsPl, prop, coords,
9      & var0, defGrad_t, defGrad,
10     & tsstif, epsZZ,
11     & var1, var2, var3, var4, var5,
12     & var6, var7, var8)
13
14
15 #include "impcom.inc"
16 #include "ansysdef.inc"
17     integer :: matId, elemId, kDomIntPt, kLayer, kSectPt, ldstep,
18     & isubst, keycut, nDirect, nShear, ncomp, nStatev, nProp
19
20
21
22     double precision :: Time, dTime, Temp, dTemp,
23     & sedEl, sedPl, epseq, epsZZ
24
25     double precision :: stress (ncomp), ustatev (nStatev),
26     & dsdePl (ncomp, ncomp), Strain (ncomp),
27     & dStrain (ncomp), epsPl (ncomp),
28     & prop (nProp), coords (3),
29     & defGrad (3,3), defGrad_t (3,3),
30     & tsstif (2)
31
32
33     EXTERNAL usermatps
34     EXTERNAL myuserfunc
35     integer :: myvar
36
37
38
39     double precision :: var0, var1, var2, var3, var4, var5,
40     & var6, var7, var8
41
42     integer :: iott, wrinqr
43     external wrinqr
44 C
45 C*****C*****C*****C*****C*****C*****C*****C*****C*****C*****
46 C
47     iott = wrinqr(WR_OUTPUT)
48     write(iott,*) '*****#DEBUG# UserMatLib.dll USERMAT'
49     write(iott,*) '#DEBUG# UserMatLib.dll USERMAT'

```

```

50   write(iott,*)'*****',myvar=99
51   call myuserfunc(myvar)
52
53
54
55
56 if ((ncomp == 3)) then
57
58
59 call usermatps (
60   & matId, elemId,kDomIntPt, kLayer, kSectPt,
61   & ldstep, isubst, keycut,
62   & nDirect, nShear, ncomp, nStatev, nProp,
63   & Time, dTime, Temp, dTemp,
64   & stress, ustatev, dsdeP1, sedEl, sedP1, epseq,
65   & Strain, dStrain, epsP1, prop, coords,
66   & var0, defGrad_t, defGrad,
67   & tsstif, epsZZ,
68   & var1, var2, var3, var4, var5,
69   & var6, var7, var8)
70
71
72 end if
73 return
74 end
75

```